to stable octahedral cobalt(IV) species at mild potentials.[12] However, the alkoxide-containing PAC ligands produce stable square-planar cobalt(III) complexes which have little affinity for axial ligands.[13] The change also presumably results from an increase in the covalent character of the in-plane σ bonding which should raise the energy of metal orbitals with axial σ symmetry and weaken the cobalt–axial ligand bonding.[20] This understanding provides a potentially valuable method for producing vacant sites in highly oxidized metal complexes.

Acknowledgment. We acknowledge the Rohm and Haas Co., the Atlantic Richfield Corp. of America, and the National Science Foundation (Grants CHE-83-11579 to F.C.A. and CHE-84-06198 to T.J.C.) for support of this work. We acknowledge Professor Paul Engel of Rice University for helpful discussions.

Supplementary Material Available: Listing of bond distances and angles and Gaussian amplitudes (4 pages); a listing of structure factor amplitudes (31 pages). Ordering information is given on any current masthead page.

(20) For a recent article discussing the occurrence of square-planar cobalt(III) complexes see: Rao, Ch. P.; Dorfman, J. R.; Holm, R. H. *Inorg. Chem.* **1986**, *25*, 428–439.

(21) *International Tables* of *X-ray Crystallography*; Kynoch Press: Birmingham, England, 1974; Vol. IV, Table 2.2B.

Molecular Structures and Electron-Transfer Kinetics for Some Pentacoordinate Cu^{I}/Cu^{II} Redox-Active Pairs

John A. Goodwin,[†] David M. Stanbury,*[†] Lon J. Wilson,*[†] C. W. Eigenbrot,[‡] and W. Robert Scheidt*[‡]

Contribution from the Department of Chemistry, William Marsh Rice University, Houston, Texas 77251, and the Department of Chemistry, University of Notre Dame, Notre Dame, Indiana 46556. *Received August 11, 1986*

Abstract: Crystal structures of the copper(I) and copper(II) complexes of the pentadentate nitrogen-bonding ligand, {bis-2,6-[1-((2-pyridin-2-ylethyl)imino)ethyl]pyridine} (= $(py)_2DAP$), $[Cu^{I}(py)_2DAP]^+$ and $[Cu^{II}(py)_2DAP]^{2+}$, have been solved as the tetrafluoroborate salts. The copper(I) complex was obtained as the hemi-methylene chloride, water solvate; the copper(II) complex was obtained as unsolvated crystals. Crystal data for $[Cu^{I}(py)_2DAP]^+$ are as follows: $CuF_4N_5C_{23}BH_{25}\cdot{}^1/_2CH_2Cl_2\cdot{}^1/_2H_2O$, $a = 15.678$ (2) Å, $b = 8.807$ (1) Å, $c = 20.727$ (2) Å, $\beta = 110.69$ (1)°, $Z = 4$, monoclinic, space group $P2/C$. Crystal data for $[Cu^{II}(py)_2DAP]^{2+}$ are as follows: $CuF_8N_5C_{23}B_2H_{25}$, $a = 11.166$ (2) Å, $b = 12.992$ (3) Å, $c = 10.364$ (2) Å, $\alpha = 106.29$ (2)°, $\beta = 109.22$ (2)°, $\gamma = 89.97$ (2)°, $Z = 2$, triclinic, space group $P\bar{1}$. Both complexes are pentacoordinate about the copper center. The copper(I) complex has an idealized trigonal bipyramidal structure with average Cu^{I}–N bond distances of 2.07 Å (trigonal plane) and 2.26 Å (axial). The coordination geometry of the copper(II) species is less regular. The average Cu^{II}–N bond distance is 0.12 Å shorter than the average Cu^{I}–N distance, but some bond lengths change substantially more than others. The kinetics of the electron self exchange for this couple has been studied in CD_3CN by dynamic NMR methods to yield a rate constant of $k'_{11} = 1.71 \times 10^3$ M^{-1} s^{-1} at 25 °C and ionic strength = 50 mM (Me_4NBF_4). The kinetics of electron cross exchange in CH_3CN has also been investigated by reducing **1**, $[Cu^{II}(py)_2DAP]^{2+}$, with two similar complexes, **2**, $[Cu^{I}(imidH)_2DAP]^+$, and **3**, $[Cu^{I}(imidR)_2DAP]^+$, and monitoring the reactions with stopped-flow techniques. The apparent rate constants at 25 °C and $\mu = 50$ mM (n-Bu_4NBF_4) are $k'_{12} = 6.44 \times 10^4$ M^{-1} s^{-1} and $k'_{13} = 6.10 \times 10^4$ M^{-1} s^{-1}. Stopped-flow studies of the ionic strength dependence indicate that ion pair formation between the copper(II) species and BF_4^- inhibits electron transfer. Under the assumption of an outer-sphere mechanism, Marcus cross relation calculations have been carried out to estimate the self-exchange rate constants for **2** and **3**. With correction of the kinetics and thermodynamics data for medium effects, these calculations have yielded $k^\circ_{22} = 1.64 \times 10^3$ M^{-1} s^{-1} and $k^\circ_{33} = 3.33 \times 10^3$ M^{-1} s^{-1} at $\mu = 0$ M, which may be compared with a value of $k^\circ_{11} = 3.05 \times 10^2$ M^{-1} s^{-1}. These electron exchange results apparently are the first to be reported for a Cu(I)/Cu(II) couple in which the coordination number is the same in the two oxidation states.

Cuproproteins involving biological redox chemistry have recently stimulated interest in deciphering relationships between the structural and electron-transfer properties of Cu(II)/Cu(I) couples at active sites.[1] Foremost among these are the blue copper proteins where X-ray crystallography has revealed active site structures with nitrogen, sulfur, and possibly oxygen donor atoms arranged around copper in tri-, tetra-, and possibly pentacoordinate geometries. In particular, plastocyanin[2] and azurin[3] have been well-studied and their relatively large self-exchange rates ($k'_{11} = 10^4$–10^6 M^{-1} s^{-1})[4,5] have been attributed to small coordination-sphere reorganization around copper during the outer-sphere Cu(II) $\rightleftarrows$ Cu(I) electron-transfer processes.[6]

One approach toward further understanding these biological electron-transfer processes is to study small molecule copper compounds of related structure and/or function. For the blue copper proteins, this "model compound" approach has been taken by others,[7] but complicating factors such as copper–ligand bond

[†] William Marsh Rice University.
[‡] University of Notre Dame.

(1) (a) *Copper Proteins*; Spiro, T. G., Ed.; Wiley: New York, **1981**. (b) *Biochemical and Inorganic Aspects of Copper Coordination Chemistry*; Karlin, K. D., Zubieta, J., Eds.; Adenine Press: **1985**. (c) *Copper Proteins and Copper Enzymes*; Lontie, R., Ed.; CRC: Boca Raton, FL, **1984**; Vols. I–III.

(2) Freeman, H. C. In *Coordination Chemistry—21*; Laurent, J. P., Ed.; Pergamon: New York, 1981; p 29–51.

(3) Norris, G. E.; Anderson, B. F.; Baker, E. N. *J. Am. Chem. Soc.* **1986**, *108*, 2784–2785.

(4) Armstrong, F. A.; Driscoll, P. C.; Hill, H. A. O. *FEBS Lett.* **1985**, *190*, 242–248.

(5) (a) Ugurbil, K.; Mitra, S. *Proc. Natl. Acad. Sci. U.S.A.* **1985**, *82*, 2039–2043. (b) Groeneveld, C. M.; Canters, G. W. *Eur. J. Biochem.* **1985**, *153*, 559–564.

(6) Gray, H. B.; Malmstrom, B. G. *Comments Inorg. Chem.* **1983**, *2*, 203–209.

0002-7863/87/1509-2979$01.50/0

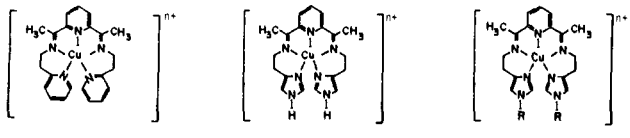

1 2 3

Figure 1. Schematic representations of the three copper complexes.

formation/rupture and potential contributory inner-sphere pathways for electron transfer have often clouded the results obtained.

Our continuing interest[8-10] in the copper chemistry of the compounds in Figure 1, has led us to investigate their electron-transfer properties in solution. Previously reported structural data for the Cu(II) form of **2** revealed it to be a pentacoordinate cation;[11] and in this work, we report that the Cu(II) and Cu(I) forms of **1** are also both pentacoordinate species. Thus, this report documents not only a rare example of a pentacoordinate copper(I) coordination compound but also its electron-transfer properties in solution where apparently there is no change in coordination number during the Cu(II) $\rightleftarrows$ Cu(I) redox chemistry. In this regard, these compounds bear on biological electron-transfer reactions, but just as importantly, they represent the first well-documented example of electron-transfer involving pentacoordinate copper(I).

Experimental Section

Materials. Acetonitrile (Burdick and Jackson) used as the reaction medium for the cross reactions was purified according to the recently developed method of Coetzee.[12] The solvent was first dried over molecular sieves (Linde, 3–4 Å porosity) before being distilled from anhydrous $CuSO_4$ and thereafter from CaH_2, with only the middle fractions being collected. Dioxygen was removed by sparging with dry argon for several hours prior to storage in a nitrogen-filled drybox (Vacuum Atmospheres Co.). Acetonitrile-d_3 used in the NMR work was Aldrich, 99% isotopic purity, and was used as received. Other solvents used in synthetic work were reagent grade or better and were used without further purification.

Supporting electrolytes, n-Bu_4NBF_4 (Aldrich), $NaBF_4$ (Alfa), and $NaBPh_4$ (Alfa), used in electrochemistry and as ionic strength media were purified by standard methods.[13,14] The electrolyte used in the NMR work, Me_4NBF_4, was prepared by neutralization of Me_4NOH with HBF_4, followed by recrystallization from water. All supporting electrolytes were dried under vacuum at 80 °C.

***N'*-(*p*-Xylyl)histamine, free base**, was prepared by the method of Merrill et al.[9]

The copper(II) complexes were synthesized, purified, and isolated according to the methods of Simmons and Merrill et al.[8,9] as described below.

{Bis-2,6-[1-((2-Imidazol-4-ylethyl)imino)ethyl]pyridine}copper(II) Bistetrafluoroborate, $[Cu^{II}(imidH)_2DAP](BF_4)_2$.[15] A ligand solution was prepared by dissolving histamine, free base (10 mmol, Sigma), and 2,6-diacetylpyridine (5 mmol, Aldrich) in methanol (150 mL) and allowing the solution to stir with reflux for $^1/_2$ h. After having cooled the yellow ligand solution to room temperature, $[Cu^{II}(H_2O)_6](BF_4)_2$ (5 mmol, Alfa) was added as a solid to the stirring solution. The resulting blue solution turned green within minutes, and the flask was stoppered and placed in the freezer to promote crystallization. After a day, the dark green crystals were collected and then recrystallized from methanol with cooling as before.

{Bis-2,6-[1-((2-pyridin-2-ylethyl)imino)ethyl]pyridine}copper(II) Bistetrafluoroborate, $[Cu^{II}(py)_2DAP](BF_4)_2$.[15] The ligand solution was prepared by dissolving 2-(2-aminoethyl)pyridine (2 mmol, Aldrich) and 2,6-diacetylpyridine (1 mmol) in methanol (50 mL) with reflux. A stoichiometric amount of solid $[Cu^{II}(H_2O)_6](BF_4)_2$ (1 mmol) was then added to the cooled solution with stirring, and the green solution was taken to dryness under reduced pressure. The resulting green solid was redissolved in acetone ($\sim$150 mL) and recrystallized over a few days with the slow addition of diethyl ether by vapor diffusion at room temperature. The crystals obtained were suitable for X-ray crystallography and were used in the structural studies as well as in the kinetic studies. Crystals were also obtained by cooling methanolic solutions; however, these were not suitable for crystallography because of their tendency to effloresce.

{Bis-2,6-[1-[((2-*N'*-*p*-xylylimidazol-4-yl)ethyl)imino]ethyl]pyridine}copper(II) Bistetrafluoroborate, $[Cu^{II}(imidR)_2DAP](BF_4)_2$.[15] A solution of 2,6-diacetylpyridine (1 mmol) and *N'*-*p*-xylylhistamine (2 mmol) in methanol (50 mL) was refluxed for 1 h and allowed to cool before solid $[Cu^{II}(H_2O)_6](BF_4)_2$ (1 mmol) was added to give the complex in solution. This solution was lyophilized, and the resulting solid was purified by chromatography of an acetone solution on a Celite filter aid column.

Tetrakis(acetonitrile)copper(I) Tetrafluoroborate, $[Cu^{I}(CH_3CN)_4](BF_4)$. This compound was prepared by the method of Simmons et al.[8] and stored in the glovebox under nitrogen.

Identity and purity of the three previously reported copper(II) complexes were confirmed by ascertaining half-wave potentials $E_{1/2}$ of the complexes by differential pulse voltammetry (DPV) of 1 mM solutions and by ^{1}H NMR of the electrochemically reduced copper(I) complexes, vide infra. These experiments were performed at a platinum wire working electrode by using a Princeton Applied Research Model 174 polarographic analyzer with an SCE reference electrode and platinum wire counter electrode. The aqueous reference electrode was separated from the bulk solution by a fritted-glass tube filled with the CH_3CN/electrolyte solution. A scan rate of 1 mV s^{-1}, modulation amplitude of 50 mV, and drop time of 1 s were used in the DPV experiments. The supporting electrolyte used was n-Bu_4NBF_4 at ca. 0.1 M. For the thermodynamic measurements with μ = 0.05 M, cyclic voltammetry (CV) at scan rates of 20 and 50 mV s^{-1} was used in the determinations of $E_{1/2}$ values, while DPV was repeated to verify reversible electrode kinetics. A BAS cell and cell stand having an electrode configuration that minimized inter-electrode distances and eliminated the bridge tube were used to reduce the problem of IR drop.

Solutions of the corresponding copper(I) complexes, which are air sensitive,[8,10] were prepared by controlled-potential bulk electrolysis in acetonitrile solution by using a cell with Schlenk-line connections. These connections allowed continuous sparging of the solution with solvent-saturated argon and also permitted collection and manipulation of the solutions. The working electrode in this cell consisted of platinum gauze, and its use allowed 100–200 mL of 0.02–1 mM solution to be prepared in times ranging from less than 1 h to ca. 3 h. A platinum wire counter electrode and an SCE reference electrode, both separated from the bulk solution by fritted-glass tubes containing electrolyte solution, completed the three-electrode geometry. The potential of the working electrode was held 240–270 mV cathodic to the measured reduction potentials of the complexes but was uncorrected for cell junction potentials in these bulk preparations. The potentiostat and coulometer used in the reductions were Princeton Applied Research Models 371 and 379, respectively. Current change was monitored with an Industrial Scientific Omniscribe strip chart recorder. Coulometry employed background compensation available on the PAR Model 379 instrument. Reduction of the copper(II) complexes has been confirmed to be a one-electron reduction process by previous work,[9] and coulometry during the present electrolyses served as a quantitative measure for completion of the reactions. For the stopped-flow kinetic experiments, stock solutions of electrochemically generated $[Cu^{I}(imidH)_2DAP]^+$ were prepared at 0.02–0.04 mM in

(7) (a) Yandell, J. In *Biochemical and Inorganic Perspectives of Copper Coordination Chemistry*; Karlin, K. D., Zubieta, J., Eds.; Adenine Press: New York, 1982; pp 157–166. (b) Rorabacher, D. B.; Martin, M. J.; Koenigbauer, M. J.; Malik, M.; Schroder, R. R.; Endicott, J. F.; Ochrymowycz, L. A.; *Ibid.* p 167–202. (c) Pulliam, E. J.; McMillin, D. R. *Inorg. Chem.* **1984**, *23*, 1172–1175.

(8) Simmons, M. G.; Merrill, C. L.; Wilson, L. J.; Bottomley, L. A.; Kadish, K. M. *J. Chem. Soc., Dalton Trans.* **1980**, 1827–1837.

(9) Merrill, C. L.; Wilson, L. J.; Thamann, T. J.; Loehr, T. M.; Ferris, N. S.; Woodruff, W. H. *J. Chem. Soc., Dalton Trans.* **1984**, 2207–2221.

(10) Goodwin, J. A.; Stanbury, D. M.; Wilson, L. J.; Scott, R. A. In *Biological and Inorganic Copper Chemistry*; Karlin, K. D., Zubieta, J., Eds.; Adenine: Guilderland, New York, 1985; Vol. II, pp 11–25.

(11) Korp, J. D.; Bernal, I.; Merrill, C. L.; Wilson, L. J. *J. Chem. Soc., Dalton Trans.* **1981**, 1951–1956.

(12) Coetzee, J. F., University of Pittsburgh, private correspondence, January 1985.

(13) Perrin, D. D.; Armarego, W. L. F.; Perrin, D. R. *Purification of Laboratory Chemicals*, 2nd ed.; Pergamon: New York, 1980; pp 528, 534.

(14) Fry, A. J.; Britton, W. E. In *Laboratory Techniques in Electroanalytical Chemistry*; Kissinger, P. T., Heineman, W. R., Eds.; Marcel Dekker: New York, 1984; p 379.

(15) This nomenclature does not follow IUPAC conventions in that the (py), (imidH), and (imidR) designations do not refer to pyridine, imidazole, and N-substituted imidazole as intact species. In all cases, diacetylpyridine (DAP) has undergone Schiff base condensation, and it also is not a discrete ligand. The compounds $[Cu(imidH)_2DAP]^{2+/+}$ and $[Cu(py)_2DAP]^{2+/+}$ have previously[8,11] had the designations $[Cu(imep)]^{2+/+}$ and $[Cu(pyep)]^{2+/+}$

Table I. Summary of Crystal Data and Intensity Collection Parameters

	$[Cu^{I}(py)_2DAP]BF_4$	$[Cu^{II}(py)_2DAP](BF_4)_2$
T, K	294	294
formula	$CuF_4N_5C_{23}BH_{25}\cdot{}^1/_2CH_2Cl_2\cdot{}^1/_2H_2O$	$CuF_8N_5C_{23}B_2H_{25}$
formula wt, amu	577.3	608.6
cryst dimensns, mm	0.09 × 0.33 × 0.31	0.74 × 0.26 × 0.29
space group	$P2/c$	$P\bar{1}$
a, Å	15.6781 (22)	11.1665 (23)
b, Å	8.8070 (11)	12.9917 (26)
c, Å	20.7270 (21)	10.3638 (22)
α, deg		106.29 (2)
β, deg	110.69 (1)	109.22 (2)
γ, deg		89.97 (2)
V, Å^3	2677.3	1355.7
Z	4	2
density (calcd) g/cm^3	1.432	1.491
density (obsd) g/cm^3		1.493
radiatn	graphite-monochromated Mo Kα (λ = 0.71073 Å)	
diffractometer	Enraf-nonius CAD4	
scan technique	θ–2θ	
ω scan range	0.80 + 0.35 (tan θ)	0.70 + 0.35 (tan θ)
2θ scan rate, deg/min	2.35–8.00	2.00–8.00
background	additional 25% on each extreme of scan	
2θ limits, deg	4.00–50.66	4.00–60.40
criterion for observtn	$F_o^2 > 3\sigma(F_o^2)$	
unique obsd data	1868	5360
μ, mm^{-1}	0.967	0.881
R_1	0.103	0.044
R_2	0.130	0.059
goodness of fit	3.41	1.96
data/parameter	9.11	12.95

18–100 mM n-Bu_4NBF_4 media immediately prior to their use and were easily maintained for the several hours during which the experiments were performed by sparging with solvent-saturated argon. This argon stream was dried with anhydrous $CaSO_4$ and scrubbed of dioxygen with a heated column of "Catalyst Q1" (finely divided copper metal on an alumina substrate, manufactured by Dow Chemical and available through Vacuum Atmospheres Co.). The electrochemical reductions of $[Cu^{II}(py)_2DAP]^{2+}$ for the NMR experiments were performed in 100 mL of CH_3CN with the amounts of materials present corresponding to those required for a 5-mL CD_3CN stock solution 5 mM in copper(I) and 35 mM in Me_4NBF_4. Preparation of the sample solutions is described in the self-exchange kinetics section.

Structure Determination. Samples of crystalline $[Cu^{I}(py)_2DAP](BF_4)\cdot{}^1/_2H_2O\cdot{}^1/_2CH_2Cl_2$ used in the crystallographic studies were obtained as follows. Reduction of the copper(II) analogue (up to 100 mg per reduction) was carried out electrochemically in acetonitrile with $NaBF_4$ as the background medium. After electrolysis, the solution was lyophilized, and the solid product dried under vacuum for 6–8 h before being transferred to a drybox. In the box, the solid was extracted with small aliquots of CH_2Cl_2 (5–10 mL each for a total volume of 50–100 mL, depending upon the amount of material reduced) to yield an orange solution of $[Cu^{I}(py)_2DAP](BF_4)$ that was treated with hexane (200–500 mL) to promote rapid precipitation of a red powder which was collected by filtration and dried under vacuum. This solid was then redissolved in a minimum volume of acetonitrile (~50 mg/100 μL), and subsequent dilution of this concentrated solution with CH_2Cl_2 and hexane (~10–20 mL each) yielded suitable crystals over 48 h, during which time the solution was kept anaerobic, at room temperature, and in the dark. The crystalline samples were transported between laboratories under nitrogen in sealed vials without refrigeration and were mounted in glass capillaries.

Preliminary examination of a red-brown crystal revealed a four-molecule monoclinic unit cell. Intensities and cell constants were measured by using an Enraf Nonius CAD4 automatic diffractometer equipped with a graphite monochromator and molybdenum X-ray tube. Least-squares refinement of the setting angles of 25 automatically centered reflections with $22° < |2\theta| < 28°$ (there were 11 ± 2θ pairs) led to the cell parameters reported in Table I. Intensity data were collected with graphite-monochromated Mo Kα radiation and θ–2θ scans. The 2θ scan rate varied from 2.35 to 8.0 deg per min. The intensities of three representative reflections were measured every 60 min of X-ray exposure. The merging R for 158 averaged reflections was 1.5% based on I. The crystal faces were identified with the help of the diffractometer, and their dimensions were measured with a binocular microscope at 30× magnification. A numerical absorption correction was applied (μ = 0.967 mm^{-1} Mo Kα). Transmission factors ranged between 0.92 and 0.75. A total of 1868 reflections with $I > 3.0\sigma(I)$ was used in the final refinement. Subsequently, an attempt was made to collect intensity data at lower temperatures. This was unsuccessful owing to a strongly temperature-dependent quasi-reversible broadening and splitting of the diffraction maxima at lower temperatures. The phenomenon is apparent at a temperature of −20 °C.

Table II. Fractional Coordinates for $[Cu^{I}(py)_2DAP]BF_4$[a]

atom	x	y	z
Cu	0.74842 (13)	0.02208 (22)	0.01401 (10)
Cl(1)	0.0308 (5)	0.4813 (10)	0.3245 (3)
N(1)	0.6477 (10)	0.1486 (16)	0.0344 (9)
N(2)	0.6316 (11)	0.0346 (17)	−0.0891 (7)
N(3)	0.7414 (8)	−0.2064 (14)	−0.0008 (6)
N(4)	0.8062 (10)	0.0907 (15)	0.1251 (7)
N(5)	0.8691 (8)	0.1124 (14)	0.0098 (6)
C(1)	0.5643 (13)	0.1756 (21)	−0.0200 (13)
C(2)	0.5005 (22)	0.269 (3)	−0.0011 (24)
C(3)	0.519 (4)	0.340 (5)	0.060 (4)
C(4)	0.5996 (20)	0.2996 (29)	0.1117 (20)
C(5)	0.6641 (16)	0.2089 (21)	0.0978 (13)
C(6)	0.7258 (12)	−0.2612 (20)	−0.0651 (9)
C(7)	0.7177 (13)	−0.4200 (23)	−0.0763 (10)
C(8)	0.7252 (13)	−0.5141 (25)	−0.0223 (11)
C(9)	0.7409 (14)	−0.4590 (25)	0.0424 (11)
C(10)	0.7498 (12)	−0.3008 (20)	0.0528 (9)
C(11)	0.9454 (11)	0.0966 (18)	0.0654 (8)
C(12)	1.0221 (13)	0.1768 (22)	0.0695 (9)
C(13)	1.0212 (13)	0.2788 (23)	0.0153 (10)
C(14)	0.9413 (14)	0.2875 (21)	−0.0427 (10)
C(15)	0.8649 (12)	0.2046 (20)	−0.0433 (9)
C(16)	0.5622 (15)	0.0942 (25)	−0.0827 (11)
C(17)	0.4578 (19)	0.078 (3)	−0.1420 (14)
C(18)	0.6379 (14)	−0.0613 (22)	−0.1436 (10)
C(19)	0.7194 (13)	−0.1529 (21)	−0.1216 (9)
C(20)	0.7537 (15)	0.1695 (22)	0.1450 (10)
C(21)	0.7799 (17)	0.2371 (28)	0.2185 (13)
C(22)	0.8996 (12)	0.0542 (20)	0.1682 (9)
C(23)	0.9446 (11)	−0.0128 (20)	0.1186 (8)
O(1)	0.5000	0.391 (4)	0.2500
O(2)	0.514 (4)	0.607 (6)	0.2766 (23)
C(24)	0.0000	0.605 (4)	0.2500

[a] The esd's of the least significant digits are given in parentheses.

The structure was solved by MULTAN82.[16] The initial E-map revealed 26 atoms of the cation. The remaining atoms were located in succeeding difference Fourier maps. Final electron density maps suggested the formulation $CuF_4N_5C_{23}BH_{29}\cdot{}^1/_2CH_2Cl_2\cdot{}^1/_2H_2O$. With Z = 4, the calculated density is 1.422 g/cm^3. The methylene chloride molecule sits on a twofold axis and is well-behaved. The oxygen atom of the water molecule was not well-behaved and was described by using two partial occupancy atoms, one on the twofold axis and the other off it. The BF_4^- ion was also poorly defined and was refined as a rigid group with B–F distances of 1.26 Å. When this refinement (using isotropic thermal parameters) reached convergence, the atoms of the BF_4^- ion were held in their derived positions, and their thermal parameters were then treated anisotropically. Sufficient data existed to refine the copper, one pyridine ring, the BF_4^- ion, and one of the water oxygen atoms with anisotropic thermal parameters. The final agreement factors are R_1 = 0.103 and R_2 = 0.130 with an error of fit of 3.41. The highest peak in the final difference Fourier map was 0.87 e/Å^3 near the water molecule. Final atomic coordinates are listed in Table II, and the associated thermal parameters are given in Table IS of the Supplementary Material.

(16) Programs used in this crystal structure study included the Enraf-Nonius SDP package and local modification of Main, Hull, Lessinger, Germain, Declerq, and Woolfson's MULTAN78, Jacobson's ALLS, Zalkin's FORDAP, Busing and Levy's ORFFE and ORFLS and Johnsons's ORTEP2. Atomic form factors were from the following: Cromer, D. T.; Waber, J. T. *International Tables of X-ray Crystallography*; Kynoch: Birmingham, England, 1974; Vol. IV, Table 2.2B. Real and imaginary corrections for anomalous dispersion in the form factor of the copper and chlorine atoms were from the following: Cromer, D. T. *International Tables of X-ray Crystallography*; Kynoch: Birmingham, England, 1974; Vol. IV, Table 2.3.1. Scattering factors for hydrogen were from the following: Stewart, R. F.; Davidson, E. R.; Simpson, W. T. *J. Chem. Phys.* **1965**, *42*, 3175–3187. All calculations were performed on a VAX 11/730.

Preliminary examination of an irregular dark green crystal of $[Cu^{II}(py)_2DAP](BF_4)_2$ grown from acetone/diethyl ether solution revealed a two-molecule triclinic unit cell. Intensity data and cell parameters were determined on the diffractometer described above. Least-squares refinement on the setting angles of 25 automatically centered reflections led to the cell parameters reported in Table I.

Intensity data were collected as described above, except that a minimum scan rate of 2.0 deg/min was used. The intensities of four representative reflections, measured every 60 min of X-ray exposure, remained constant within experimental error during the 192.2 h of data collection. Azimuthal scans of six reflections with 2θ between 15 and 34° all had ratios of I_{min}/I_{max} of approximately 0.77. Because of the irregular shape of the crystal, an empirical absorption correction was applied (μ = 0.881 mm^{-1} Mo Kα). Normalized transmission coefficients ranged between 1.00 and 0.78. The merging R for 596 averaged reflections was 1.1% based on I. A total of 5360 reflections with $I > 3.0\sigma(I)$ were used in the final refinement.

The structure was solved by using MULTAN82. The initial E-map revealed 15 atoms of the cation. The remaining atoms were located in succeeding difference Fourier maps. Both the BF_4^- anions are disordered. One exhibits disorder about a local threefold axis and was described with one boron and seven fluorine atoms. The ratio of the occupancies of the disordered fluorines was set to 78/22. The other anion was described with one boron and eight fluorine atoms. The ratio of disordered fluorines was set to 63/37. Most of the expected hydrogen atoms were revealed in the difference maps. These atoms were included in calculated idealized positions (C–H = 0.95 Å) with isotropic temperature factors of 6.0 $Å^2$ and as fixed contributors in all successive cycles of least-squares refinement. All heavy atoms were included with anisotropic thermal parameters. Final agreement factors are R_1 = 0.044 and R_2 = 0.059 with an error fit of 1.96. The highest peak in the final difference map was 0.44 e/$Å^3$ and was near the copper ion. Final atomic coordinates are listed in Table III, and the associated thermal parameters appear in Table IIIS of the Supplementary Material.

Conductivity Experiments. A standard conductivity cell (Fisher, medium range, cell constant, k = 1.473 cm^{-1}) was modified by adding a glass reservoir which allowed the cell compartment concentrations to be varied by adding aliquots of concentrated solution. The platinum electrodes were freshly platinized prior to use. A YSI model 31 conductivity bridge operating at 1 kHz was used for all measurements. Temperature was maintained at 25 °C by a Blue M, MagniWhirl regulated oil bath. Solutions were prepared in the drybox from solids weighed on a microgram balance; freshly distilled CH_3CN was used. The conductivity cell and stock solution were maintained under a dry atmosphere by blanketing the solutions with solvent-saturated argon. Additions of the stock solution were by standard syringe techniques. The errors in measurement are estimated to be ±10%.

Cross-Exchange Stoichiometry. Absorption spectra of the product solutions were taken anaerobically by using a Cary 210 UV–vis spectrophotometer and matched quartz cells having a 1-cm pathlength and fitted with stopcocks to allow anaerobic handling and measurement. Isomolar solutions of varying proportions of reactants were prepared, and their visible-wavelength spectra were recorded. Visible-wavelength absorption spectra of the proposed products were compared to spectra of samples previously prepared by synthetic methods.

Cross-Exchange Kinetics. The moderately fast electron-transfer reactions involving the $[Cu^{II}(py)_2DAP]^{2+}$ cation with both $[Cu^{I}(imidH)_2DAP]^+$ and $[Cu^{I}(imidR)_2DAP]^+$ were monitored by observing the small changes in absorbance associated with the difference in reactant and product copper(I) spectra. This change in absorbance was greatest at 355 nm for eq 2 and for the experimental conditions given below, ΔA = 0.025. For eq 3, it was necessary to double the concentration of the reactant copper(I) species in comparison to the concentration used in eq 2, and even with this advantage, the ΔA value was only 0.014 or close to the limits of detection. An Aminco–Morrow stopped-flow device equipped with an OLIS 3820 data collection system and having a pathlength of 1 cm was used for data collection. Typical concentrations of the Cu(I) species were 10^{-5} M while those of the Cu(II) species were at least 10-fold greater. The absorbance changes were routinely signal averaged over 4–8 shots, and the log $(A_\infty - A_t)$ of the mean values were plotted vs. time. Fits to linearity were made for these plots by using data reduction routines available in the OLIS system. In general, these plots were linear over the span of $2^1/_2$–4 half-lives.

Ion pairing of the supporting electrolyte, n-Bu_4NBF_4, was taken into account in treating the data. The effective ionic strengths, calculated with an ion-association constant for n-Bu_4NBF_4 of K_{IP} = 10 M^{-1}, were used throughout this work.[17] All experiments were performed at a constant ionic strength of μ = 9.0 mM, except for those instances in which it was systematically varied from 1.8 to 52 mM. The sample temperature of the stopped-flow experiments was maintained at 25.0 °C (±0.05°) by using a Lauda K-2/R thermostated bath which circulated water around the mixing chamber.

A flow of nitrogen gas around the exterior of the mixing compartment of the stopped-flow instrument alleviated problems associated with air diffusion through the Teflon tubing which connected the drive syringes and the sample cell in the apparatus. All manipulations were made with standard syringe techniques (glass syringes and stainless steel needles) with the added precaution of using Teflon and Nylon syringe stopcocks to keep the system anaerobic. A solvent-saturated argon line, as described above, was used to keep all stock solutions dry and free of dioxygen. Without these added precautions, the reaction rate gradually increased with the residence time of the sample solution in the drive syringes due to diffusion of air.

Other substances, particularly dioxygen, water, and $[Cu^{I}(CH_3CN)_4](BF_4)$, were added to the sample solutions to check for their effects on the reactions, since they were considered the most likely contaminants. The $[Cu^{I}(CH_3CN)_4]^+$ solutions were prepared volumetrically in the drybox and added in concentrations ranging from 10^{-5}–10^{-4} M. Water solutions were prepared volumetrically on the argon line immediately prior to use, and the concentrations were similar to those used for $[Cu^{I}(CH_3CN)_4]^+$. The effect of dioxygen was ascertained by using Cu(I) sample solutions saturated in dioxygen with variable delay times between dioxygen exposure and stopped-flow mixing.

The anion substitution experiments used volumetrically prepared solutions of $NaBPh_4$ added to the solutions of the BF_4^- salts of the copper complexes. The $NaBPh_4$ was added in quantities that gave the BPh_4^- ion

Table III. Fractional Coordinates for $[Cu^{II}(py)_2DAP](BF_4)_2$[a]

atom	x	y	z
Cu	0.219568 (28)	0.287175 (22)	0.18459 (3)
N(1)	0.34521 (18)	0.40627 (15)	0.23681 (20)
N(2)	0.33423 (23)	0.21889 (17)	0.07757 (21)
N(3)	0.06348 (22)	0.21886 (19)	0.00960 (23)
N(4)	0.15449 (19)	0.40313 (15)	0.31410 (22)
N(5)	0.22841 (21)	0.19934 (15)	0.33221 (21)
C(1)	0.43818 (23)	0.39188 (21)	0.18169 (26)
C(2)	0.52877 (28)	0.47546 (27)	0.2151 (3)
C(3)	0.5188 (3)	0.57405 (27)	0.3049 (4)
C(4)	0.4204 (3)	0.58821 (23)	0.3587 (4)
C(5)	0.33234 (24)	0.50086 (20)	0.32139 (26)
C(6)	0.0681 (4)	0.12044 (26)	−0.0778 (3)
C(7)	−0.0275 (6)	0.0812 (4)	−0.2110 (4)
C(8)	−0.1259 (7)	0.1391 (6)	−0.2526 (6)
C(9)	−0.1289 (4)	0.2375 (5)	−0.1616 (6)
C(10)	−0.0331 (3)	0.2760 (3)	−0.0323 (4)
C(11)	0.13815 (28)	0.20845 (19)	0.39403 (28)
C(12)	0.1558 (4)	0.17313 (26)	0.5126 (4)
C(13)	0.2631 (5)	0.1261 (3)	0.5641 (4)
C(14)	0.3538 (4)	0.11653 (28)	0.5007 (4)
C(15)	0.3339 (3)	0.15389 (23)	0.3864 (3)
C(16)	0.42480 (26)	0.28030 (23)	0.08364 (26)
C(17)	0.5119 (3)	0.2521 (3)	−0.0014 (3)
C(18)	0.3044 (4)	0.10759 (26)	−0.0188 (3)
C(19)	0.1772 (4)	0.05887 (24)	−0.0272 (3)
C(20)	0.21993 (24)	0.49464 (19)	0.36695 (28)
C(21)	0.1934 (3)	0.59001 (24)	0.4694 (4)
C(22)	0.04913 (26)	0.38074 (23)	0.3620 (3)
C(23)	0.02223 (28)	0.25996 (23)	0.3309 (3)
B(1)	0.6564 (4)	0.12377 (29)	0.3312 (4)
F(1a)	0.6467 (4)	0.1556 (4)	0.4650 (5)
F(2)	0.56994 (22)	0.03727 (18)	0.24751 (26)
F(3a)	0.6365 (7)	0.2072 (5)	0.2786 (7)
F(4a)	0.7771 (4)	0.0933 (3)	0.3479 (5)
F(1b)	0.7478 (23)	0.1339 (14)	0.298 (4)
F(3b)	0.683 (3)	0.1322 (20)	0.4602 (22)
F(4b)	0.5951 (10)	0.2168 (9)	0.3244 (16)
B(2)	0.1776 (4)	0.4373 (4)	0.8453 (5)
F(5a)	0.1788 (3)	0.4456 (4)	0.7153 (4)
F(6a)	0.0562 (4)	0.4448 (5)	0.8403 (8)
F(7a)	0.2248 (9)	0.3487 (7)	0.8616 (9)
F(8a)	0.2490 (6)	0.5190 (7)	0.9498 (6)
F(5b)	0.2077 (7)	0.5374 (8)	0.8336 (15)
F(6b)	0.1625 (9)	0.4603 (8)	0.9780 (8)
F(7b)	0.0750 (9)	0.3792 (11)	0.7517 (12)
F(8b)	0.2811 (9)	0.3793 (10)	0.8502 (14)

[a] The esd's of the least significant digits are given in parentheses.

(17) Nielson, R. M.; Wherland, S. *Inorg. Chem.* **1984**, *23*, 1338–1344. This paper reports that association for $[Mn(CNC_6H_{11})_6](BF_4)_2$ is "small".

Table IV. Bond Distances for $[Cu^I(py)_2DAP]BF_4$ and $[Cu^{II}(py)_2DAP](BF_4)_2$ (Å)[b]

bond	Cu^I	Cu^{II}	bond	Cu^I	Cu^{II}
Cu–N(1)	2.094 (14)	1.920 (2)	N(1)–C(1)	1.413 (22)	1.330 (3)
Cu–N(2)	2.273 (14)	2.010 (2)	N(1)–C(5)	1.354 (23)	1.333 (3)
Cu–N(3)	2.032 (12)	2.033 (2)	N(2)–C(16)	1.255 (22)	1.263 (4)
Cu–N(4)	2.240 (14)	2.026 (2)	N(2)–C(18)	1.442 (21)	1.473 (4)
Cu–N(5)	2.083 (12)	2.129 (2)	N(3)–C(6)	1.356 (19)	1.356 (4)
N(5)–C(11)	1.343 (18)	1.350 (3)	N(3)–C(10)	1.356 (19)	1.332 (4)
N(5)–C(15)	1.350 (19)	1.342 (4)	N(4)–C(20)	1.253 (21)	1.272 (3)
C(1)–C(2)	1.45 (3)	1.372 (4)	N(4)–C(22)	1.455 (20)	1.477 (3)
C(1)–C(16)	1.474 (27)	1.493 (4)	C(6)–C(7)	1.415 (22)	1.393 (5)
C(2)–C(3)	1.34 (8)	1.385 (4)	C(6)–C(19)	1.486 (23)	1.487 (5)
C(3)–C(4)	1.38 (8)	1.376 (5)	C(7)–C(8)	1.364 (24)	1.353 (8)
C(4)–C(5)	1.396 (27)	1.382 (4)	C(8)–C(9)	1.365 (26)	1.367 (9)
C(11)–C(12)	1.371 (22)	1.385 (4)	C(9)–C(10)	1.409 (24)	1.368 (5)
C(11)–C(23)	1.469 (21)	1.496 (4)	C(16)–C(17)	1.67 (3)	1.500 (4)
C(12)–C(13)	1.435 (24)	1.362 (6)	C(18)–C(19)	1.443 (23)	1.522 (5)
C(13)–C(14)	1.399 (24)	1.366 (6)	C(20)–C(21)	1.550 (27)	1.489 (4)
C(14)–C(15)	1.399 (23)	1.356 (4)	C(22)–C(23)	1.554 (22)	1.520 (4)
C(24)–Cl	1.810 (22)		C(20)–C(5)	1.443 (26)	1.489 (3)
B–F(3)	1.578		B–F(1)[a]	1.397	
B–F(4)	1.393		B–F(2)	1.362	
B(1)–F(1a)		1.520 (5)	B(2)–F(5a)		1.540 (5)
B(1)–F(2)		1.523 (4)	B(2)–F(6a)		1.556 (6)
B(1)–F(3a)		1.603 (6)	B(2)–F(7a)		1.552 (8)
B(1)–F(4a)		1.519 (6)	B(2)–F(8a)		1.533 (6)
B(1)–F(1b)		1.550 (26)	B(2)–F(5b)		1.579 (8)
B(1)–F(3b)		1.592 (25)	B(2)–F(6b)		1.563 (8)
B(1)–F(4b)		1.530 (12)	B(2)–F(7b)		1.540 (10)
			B(2)–F(8b)		1.540 (11)

[a] All boron–fluorine distances are corrected for thermal motion. [b] The esd's of the least significant digits are given in parentheses.

a 10-fold excess in concentration over the BF_4^- ion.

NMR Experiments. Proton magnetic resonance spectra and Carr–Purcell–Mieboom–Gill T_2 measurements were obtained with an IBM 300-MHz NMR spectrometer operating at 300.13 MHz with a frequency bandwidth of 3311 Hz described by 32K data points. Presaturation homonuclear spin decoupling was employed by irradiating the α-methylene (α to the imino nitrogen atom) resonance at 4.11 ppm for 3 s prior to the 5-s observation. For the line-broadening measurements, two spectra were recorded to estimate the limits of experimental error. In general, these differed by the number of time domain accumulations, specifically, 16 and 75. An exponential window function introduced line broadening of 0.50 Hz, and this contribution was taken into account in the line-broadening measurements. Samples were spun at 30 Hz and maintained at ambient temperature (ca. 27 °C).

The NMR samples of $[Cu^I(py)_2DAP](BF_4)$ were electrochemically generated in CH_3CN as described in the synthesis section. These electrolysis solutions were lyophilized and dried under vacuum for 6–8 hours before being transferred into the drybox for preparation of the 5-mL CD_3CN stock solution and subsequent sample preparation. Since the bulk electrolysis required an excess of supporting electrolyte (a sevenfold molar excess was used) and because the corresponding concentration of the copper complex needed to be as large as possible for adequate detection by NMR, Me_4NBF_4 was chosen as the supporting electrolyte. Although the sodium salt was preferred because of the lack of spectral complications it would have introduced, it had insufficient solubility for these experiments. The methylammonium salt was chosen instead of higher alkylammonium homologues because of the relative simplicity of its proton NMR spectrum.

All samples for the measurement of $1/T_2$ dependence upon $[Cu^{II}(py)_2DAP]^{2+}$ concentration were prepared in the same 5-mm sample tube (Wilmad, "Emperor" Grade, fitted with a silicone septum, a Teflon liner, and a screw cap). To the first sample, which contained only $[Cu^I(py)_2DAP](BF_4)$ and Me_4NBF_4, a concentrated solution of $[Cu^{II}(py)_2DAP]^{2+}$ was added. To maintain the concentration of the copper(I) species and ionic strength, this copper(II) solution contained $[Cu^I(py)_2DAP]^+$ and Me_4NBF_4 at the same concentrations as in the sample containing only copper(I). The copper(II) stock solution was added via an air-tight syringe.

Numerical Methods. Kinetics data analyses were carried out by using the Los Alamos Nonlinear Least Squares Program. Unit weighting was used in the ionic strength dependence studies. The linear fits of the dependence of the cross- and self-exchange rates upon the concentrations of the unobserved and major species used weighting inverse to the dependent variable.

Results

Crystal Structures. An overall perspective view of the $[Cu^I(py)_2DAP]^+$ cation, as given in Figure 2A, illustrates the atom labeling scheme and the bond distances in the coordination group cation. Individual values of bond distances and angles are given in Tables IV and V, respectively. The coordination sphere of the $[Cu^I(py)_2DAP]^+$ cation is best described as trigonal bipyramidal with the three pyridine nitrogen atoms defining the trigonal plane. The three angles in this plane are close to the ideal 120°; N(1)CuN(3) and N(1)CuN(5) are 123.6 (5) and 124.5 (5)°, and N(3)CuN(5) is 111.9 (5)°. The Cu(I) ion is only 0.02 Å out of the trigonal plane. The angle between the "axial" ligands, the two imino nitrogen atoms, is 148.5 (6)°, significantly less than the ideal value of 180°. The average bond distance to the three trigonal pyridine donor atoms is 2.070 (33) Å. The average bond distance to the two axial imino donor atoms is substantially longer at 2.257 (23) Å. Thus the equatorial donor atoms interact much more strongly with the Cu(I) ion than the axial donors. Finally it should be noted that the features of the coordination group are much closer to the expected C_2 symmetry than that found for the related Cu(II) complex, vide infra. The idealized C_2 axis of the coordination group includes the central pyridine ring and the Cu–N(1) bond. The idealized C_2 symmetry of $[Cu^I(py)_2DAP]^+$ is the maximum symmetry that this intrinsically chiral complex can possess. However, both $[Cu^I(py)_2DAP]^+$ and $[Cu^{II}(py)_2DAP]^+$ crystallize in centrosymmetric space groups and exists as enantiomeric pairs in the solid. Deviations from selected least-squares planes and the dihedral angles between these planes are given in Table VI.

Figure 2B gives an overall perspective view of the $[Cu^{II}(py)_2DAP]^{2+}$ cation. The figure clearly indicates the pentacoordinate nature of the ion. This figure has the same general molecular orientation as that presented in Figure 2A for the copper(I) cation and illustrates the atom labeling scheme and the bond distances in the coordination cation. Individual values of bond distances and bond angles are given in Tables IV and V, respectively.

Conductivity Measurements. In an attempt to establish the association constant, K_{IP1}, for $[Cu^{II}(py)_2DAP]^{2+}$ with BF_4^-, independently of the kinetic studies, conductivity measurements were performed on solutions of $[Cu^{II}(py)_2DAP](BF_4)_2$. The concentrations ranged from 0.1 to 2.0 mM. The data were analyzed by

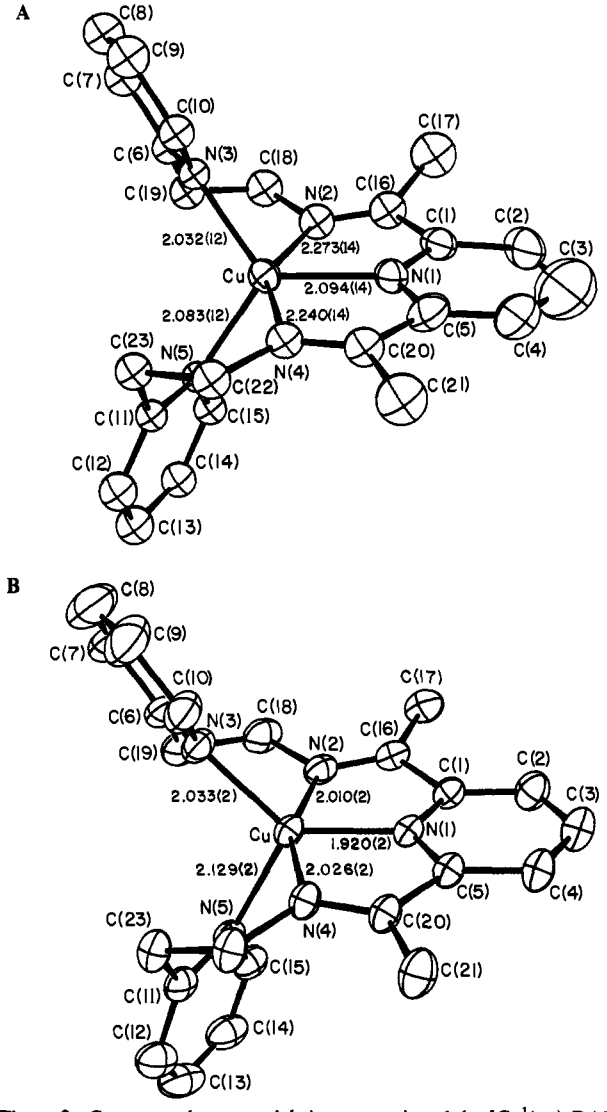

Figure 2. Computer-drawn models in perspective of the $[Cu^{I}(py)_2DAP]^+$ cation, A, and of the $[Cu^{II}(py)_2DAP]^{2+}$ cation, B, as they exist in the crystalline phase. The atom labeling scheme and bond distances in the coordination group are also displayed. Ellipsoids are contoured at the 20% probability level in both.

constructing plots of Λ_{eq} vs. $c^{1/2}$ and comparing them with theoretically generated curves. To obtain these curves, the Fuoss–Edelson[18] equation for 2:1 electrolytes was solved for Λ_{eq} in terms of $c^{1/2}$ to give

$$\Lambda_{eq} = \gamma_1(\lambda^\circ_1 + \lambda^\circ_2 + c^{1/2}(\alpha_3 - \alpha_1 - 2\alpha_2)) + (\alpha_2 - \alpha_3)\alpha_3 c^{1/2} \quad (1)$$

A modification to the original derivation was made; i.e., $\lambda_2^\circ = \lambda_3^\circ$, not $\lambda_2^\circ = 2\lambda_3^\circ$, since *equivalent* conductivities are considered. The variables in eq 1 are defined in ref 18. Λ_{eq}° was estimated by extrapolating a plot of Λ_{eq} to $c^{1/2} = 0$, and assumed values of K_{IP1} were varied systematically from 0 to 1000 M^{-1}. Comparison of the experimental and theoretical results yielded an approximate value for K_{IP1} of 300 ± 200 M^{-1}. The level of uncertainty in this result is larger than customarily found for 1:1 electrolytes, because for a 2:1 electrolyte the conductivity differs by only a factor of 2 between the free ions and the fully ion-paired species, whereas for a 1:1 electrolyte the fully ion-paired species has no conductivity. Similar measurements of the conductivity for $[Cu^{II}(imidH)_2DAP](BF_4)_2$ were also used to obtain a K_{IP2} value of 100 ± 25 M^{-1}.

(18) Fuoss, R. M.; Edelson, D. *J. Am. Chem. Soc.* **1951**, *73*, 269–273.

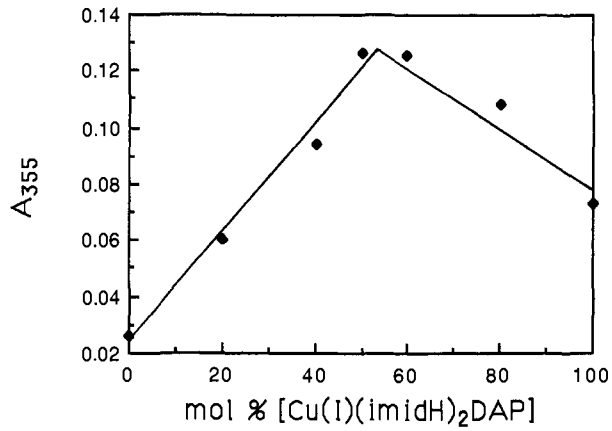

Figure 3. Job plot for eq 2, where total concentration, M = 0.08 mM, $\lambda_{max\Delta}$ = 355 nm, and μ = 0.01 M (n-Bu_4NBF_4); measurement performed anaerobically.

Reaction Stoichiometry. The reactions chosen for study in the stopped-flow work are given in eq 2 and 3 as

$$\underset{\mathbf{1}}{[Cu^{II}(py)_2DAP]^{2+}} + \underset{\mathbf{2}}{[Cu^{I}(imidH)_2DAP]^+} \rightarrow [Cu^{I}(py)_2DAP]^+ + [Cu^{II}(imidH)_2DAP]^{2+} \quad (2)$$

$$\underset{\mathbf{1}}{[Cu^{II}(py)_2DAP]^{2+}} + \underset{\mathbf{3}}{[Cu^{I}(imidR)_2DAP]^+} \rightarrow [Cu^{I}(py)_2DAP]^+ + [Cu^{II}(imidR)_2DAP]^{2+} \quad (3)$$

where the labels for the individual complexes correspond to the labels in Figure 1 and to the subscript designations used throughout this paper. The Job plot, constructed for eq 2 and shown in Figure 3, was obtained from the product mixture absorption values for a series of isomolar solutions at 355 nm, the wavelength at which the largest absorption change occurs during the reaction. Job's method of isomolar solutions was developed for the study of complex formation stoichiometries with reactions of the type A + bB ⇌ AB_b,[19] but it can be shown that it also applies to reactions with the general stoichiometry aA + bB → products. Figure 3 shows a change in slope at $a/(a + b) \approx 0.5$, which implies that the two copper complexes react in a 1:1 ratio.

Product solution spectra were also compared with spectra obtained by summing the spectra of the proposed products. These spectra are illustrated in Figure 4, and the excellent agreement between the actual spectra and the summation spectra strongly supports the reaction stoichiometry given in eq 2 and 3.

Equilibrium quotients for these two reactions were obtained from the half-wave potentials for each of the copper complex couples at μ = 0.038 M. These values, listed in Table VIII, lead to values for K_{12} and K_{13} of 178 and 107, respectively, for eq 2 and 3. This implies that the reactions proceed to at least 99% completion in the kinetics studies described below.

Cross-Exchange Kinetics. The stopped-flow experiments were performed by maintaining the oxidant in large excess in order to attain pseudo-first-order conditions as well as to minimize the effects of dioxygen contamination. Table IX lists the pseudo-first order rate constants, k_{obsd}, obtained at μ = 9.0 mM. The first-order dependence of the rate upon the concentration of $[Cu^{I}(imidH)_2DAP]^+$ was verified for eq 2 by the invariance of the pseudo-first-order rate constants across varied initial concentrations of the minor copper(I) species. Plots of k_{obsd} vs. the concentration of the copper(II) complex are shown in Figure 5A and B. The linearity of these plots indicates a first-order dependence on $[Cu^{II}]$. Least-squares fits to the data of a linear function yield apparent second-order rate constants of k_{12} = 2.39 ± 0.08 × 10^4 M^{-1} s^{-1} and k_{13} = 1.71 ± 0.11 × 10^4 M^{-1} s^{-1}. In these fits, the intercepts were not constrained to zero; for eq 2, the intercept was 0.23 ±

(19) Drago, R. S. *Physical Methods in Chemistry*; W. B. Saunders: Philadelphia, 1977; p 255 and references therein.

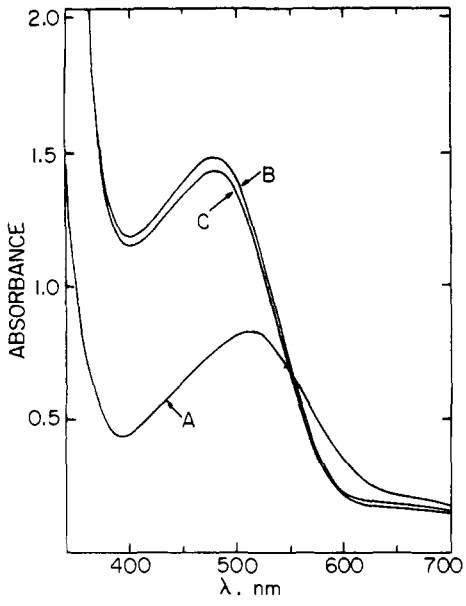

Figure 4. Electronic spectra for eq 2. A. Unmixed solution of reactants $[Cu^{I}(imidH)_2DAP]^+$, 0.5 mM, and $[Cu^{II}(py)_2DAP]^{2+}$, 0.5 mM in CH_3CN. The different solutions were contained in separate 1-cm pathlength quartz cells which were placed in the spectrophotometer beam simultaneously. B. Product solution of the mixed reactants at the same concentrations of A. A second 1-cm cell containing only electrolyte solution was also placed in the beam to compensate for its absorbance for comparison to A and C. C. Proposed product spectrum obtained by placing one 1-cm cell containing electrochemically reduced $[Cu^{I}(py)_2DAP]^+$, 0.5 mM, and another 1-cm cell containing $[Cu^{II}(imidH)_2DAP]^{2+}$, 0.5 mM, in the spectrophotometer beam. Concentration of n-Bu_4NBF_4 in all solutions is 50 mM. All solutions containing reduced species were handled under rigorously anaerobic conditions.

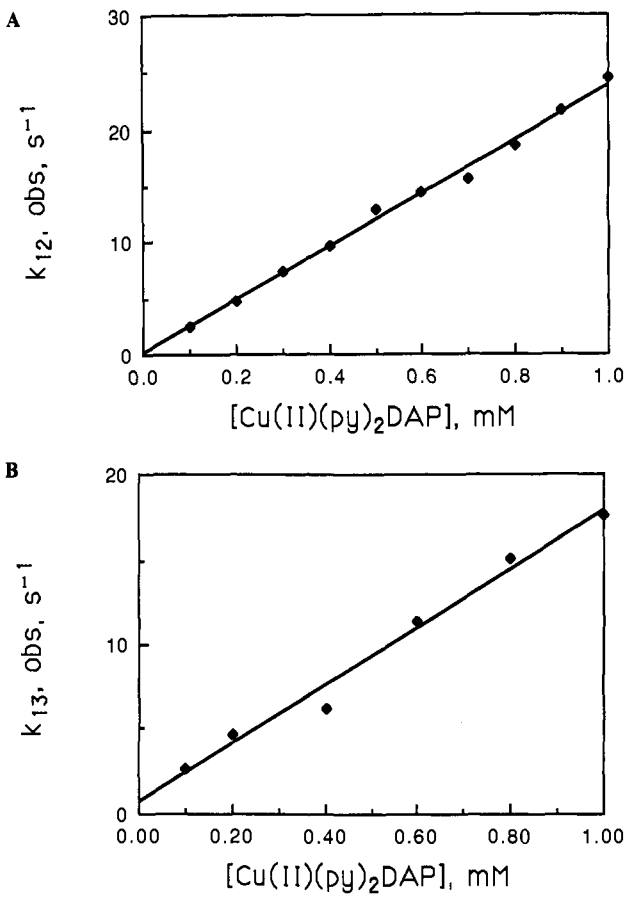

Figure 5. Dependence of pseudo-first-order rate constants of electron transfer upon concentration of the major species: A. Variation of $[Cu^{II}(py)_2DAP]^{2+}$ concentration in oxidation of $[Cu^{I}(imidH)_2DAP]^+$. B. Variation of $[Cu^{II}(py)_2DAP]^{2+}$ concentration in oxidation of $[Cu^{I}(imidR)_2DAP]^+$. Both reactions were in CH_3CN at 25.0 °C with μ = 0.01 M (n-Bu_4NBF_4) and were measured anaerobically.

0.4 s^{-1}, and for eq 3, it was 0.77 ± 0.64 s^{-1}. Thus, both intercepts were statistically insignificant.

Deliberate addition of dioxygen for eq 2 enhanced the rate of reaction, and pseudo-first-order rate constants with values up to 60 s^{-1} were obtained at oxidant concentrations of 0.2 mM, which may be compared to the anaerobic rate constant of 4.8 s^{-1}. Additions of $[Cu^{I}(CH_3CN)_4]^+$ and water, on the other hand, did not enhance the reaction rate. Interestingly, in reactions in which either of the latter two substances was added in the presence of dioxygen, the rate enhancement by dioxygen was apparently quenched. These effects are not presently understood, but in light of the fascinating dioxygen reactivity[9] of $[Cu^{I}(imidH)_2DAP]^+$ and $[Cu^{I}(imidR)_2DAP]^+$ more detailed studies in that regard seem warranted. For the present studies, water and $[Cu^{I}(CH_3CH)_4]^+$ were excluded, and anaerobicity was maintained rigorously.

The ionic strength dependence for the cross-reactions was measured by varying μ from 1.8 to 52 mM. These data are listed in Table IX. The variations in the rate constants, k_{12} and k_{13}, observed in these experiments were treated by three methods. The first treatment assumes a simple second-order rate law, where the rate constant varies according to the Debye–Hückel expression, given as

$$\log k = \log k^\circ + (\Delta z^2)^\ddagger A\mu^{1/2}/(1 + Ba\mu^{1/2}) \qquad (4)$$

where $B = (8\pi Ne^2/1000\epsilon k_B T)^{1/2} = 0.486\ M^{-1/2}\ Å^{-1}$,[20] and a is the ion size parameter maintained at 3.5 Å.[21] The value for ϵ is 35.95,[22] and k_B is the Boltzman constant. In the absence of other effects, a plot of log k vs. $(\mu^{1/2})/(1 + Ba\mu^{1/2})$ for a system of the ionic reactants having charges of z_1 and z_2 should be linear with the slope corresponding to the $(\Delta z^2)^\ddagger A$ term in eq 4 (here equal to $2z_1z_2A$). Figure 6 shows plots of log k_{12} and log k_{13} vs. $(\mu^{1/2})/(1 + Ba\mu^{1/2})$. The least-squares slope for eq 2 is 5.63 ± 0.34, and for eq 3 it is 4.70 ± 0.18. Since the theoretical value of A for CH_3CN at 25 °C is 1.646 $M^{-1/2}$ (base ten logarithms), the $(\Delta z^2)^\ddagger$ terms for the two reactions take on values of 3.42 and 2.85 for eq 2 and 3, respectively. Because the theoretical value of $(\Delta z^2)^\ddagger$ is 4 for the system where $z_1 = +1$ and $z_2 = +2$, it is apparent that neither reaction is well-described by this simple model.

In view of the substantial ion pairing indicated by the conductivity studies, a more sophisticated treatment of the ionic strength dependence was considered. It assumes that ion pairing is significant only for Cu(II), and that only the free complexes are reactive. This leads to

$$k_{obsd} = k_a[Cu^{II}L]/(1 + K_{IP1}[BF_4^-]) \qquad (5)$$

where k_a is the bimolecular rate constant. A third approach also includes a pathway for reaction of the ion-paired species, and this leads to

$$k_{obsd} = (k_b + k_cK_{IP1}[BF_4^-])[Cu^{II}L]/(1 + K_{IP1}[BF_4^-]) \qquad (6)$$

where k_b is analogous to k_a in eq 5, and k_c is the rate constant

(20) Bockris, J. O'M.; Reddy, A. K. M. *Modern Electrochemistry*; Plenum: New York, 1973; Vol. 1, p 210.

(21) Estimated from the values for several $[Bu_4N]^+$ salts in CH_3CN given in Fernandez-Prini, R. In *Physical Chemistry of Organic Solvent Systems*; Covington, A. K., Dickenson, T., Eds.; Plenum: London, 1973. The values for $[Bu_4N]Br$ (3.5 Å), $[Bu_4N]ClO_4$ (3.57 Å), $[Bu_4N]NO_3$ (3.73 Å), and $[Bu_4N]I$ (3.6 Å) were relatively independent of the anion, while the values of $[Bu_4N]Pic$ (4.0 Å) and $[Bu_4N]BPh_4$ (4.5 Å) deviate because of their bulk. Clearly, the relatively small BF_4^- salt would fall into the first category. Variations in size of $[R_4N]^+$ cation led to slightly greater variations in the ion size parameter. The reported value of a for $NaBPh_4$ is 5.2 Å.

(22) (a) Robinson, R. A.; Stokes, R. H. *Electrolyte Solutions*; 2nd ed.; Academic: New York, 1959; p 230. (b) Coetzee, J. F.; Martin, M. W. In *Recommended Methods for Purification of Solvents*; Coetzee, J. F., Ed.; Pergamon: New York, 1982; pp 10–15.

Table V. Bond Angles for $[Cu^{I}(py)_2DAP]BF_4$ and $[Cu^{II}(py)_2DAP](BF_4)_2$ (deg)[a]

angle	Cu^{I}	Cu^{II}	angle	Cu^{I}	Cu^{II}
N(1)-Cu-N(2)	75.5 (6)	79.18 (9)	C(1)-N(1)-C(5)	120.9 (18)	122.87 (22)
N(1)-Cu-N(3)	123.6 (5)	134.42 (8)	N(1)-C(1)-C(2)	114.2 (26)	120.06 (25)
N(1)-Cu-N(4)	73.1 (6)	79.09 (8)	N(1)-C(1)-C(16)	110.3 (17)	111.54 (22)
N(1)-Cu-N(5)	124.5 (5)	119.53 (8)	C(2)-C(1)-C(16)	135.3 (27)	128.39 (24)
N(2)-Cu-N(3)	85.6 (5)	90.45 (10)	C(1)-C(2)-C(3)	125. (4)	118.11 (26)
N(2)-Cu-N(4)	148.5 (6)	158.27 (9)	C(2)-C(3)-C(4)	116.7 (29)	121.10 (27)
N(2)-Cu-N(5)	112.6 (5)	105.48 (8)	C(3)-C(4)-C(5)	121. (4)	118.06 (28)
N(3)-Cu-N(4)	113.8 (5)	105.04 (10)	C(4)-C(5)-N(1)	121.5 (26)	119.76 (24)
N(3)-Cu-N(5)	111.9 (5)	106.04 (9)	C(4)-C(5)-C(20)	126.8 (27)	128.46 (25)
N(4)-Cu-N(5)	84.1 (5)	85.10 (8)	N(1)-C(5)-C(20)	111.7 (17)	111.76 (21)
C(6)-N(3)-C(10)	121.2 (4)	119.60 (27)	C(11)-N(5)-C(15)	122.3 (14)	118.76 (22)
N(3)-C(6)-C(7)	119.2 (16)	119.4 (4)	N(5)-C(11)-C(12)	119.7 (16)	120.31 (29)
N(3)-C(6)-C(19)	119.0 (16)	118.07 (25)	N(5)-C(11)-C(23)	118.1 (15)	117.15 (22)
C(7)-C(6)-C(19)	121.8 (17)	122.5 (4)	C(12)-C(11)-C(23)	122.1 (16)	122.53 (27)
C(6)-C(7)-C(8)	119.3 (19)	120.7 (5)	C(11)-C(12)-C(13)	120.5 (17)	119.6 (3)
C(7)-C(8)-C(9)	121.5 (21)	118.5 (4)	C(12)-C(13)-C(14)	117.7 (19)	119.90 (29)
C(8)-C(9)-C(10)	118.4 (20)	120.1 (5)	C(13)-C(14)-C(15)	118.9 (18)	118.7 (3)
C(9)-C(10)-N(3)	120.3 (17)	121.6 (4)	C(14)-C(15)-N(5)	120.8 (16)	122.8 (3)
C(1)-C(16)-C(17)	113.6 (19)	119.48 (27)	C(16)-N(2)-C(18)	129.0 (18)	121.28 (25)
C(1)-C(16)-N(2)	123.1 (20)	114.36 (21)	N(2)-C(18)-C(19)	112.3 (17)	110.56 (25)
N(2)-C(16)-C(17)	123.1 (21)	126.09 (28)	C(18)-C(19)-C(6)	114.4 (16)	113.85 (28)
C(5)-C(20)-N(4)	120.4 (19)	114.57 (22)	C(20)-N(4)-C(22)	123.8 (16)	120.81 (22)
C(5)-C(20)-C(21)	115.5 (20)	120.23 (23)	N(4)-C(22)-C(23)	105.8 (14)	109.99 (21)
N(4)-C(20)-C(21)	124.0 (20)	125.18 (24)	C(22)-C(23)-C(11)	111.9 (14)	112.75 (23)
F(1a)-B(1)-F(2)		109.2 (4)	Cl(1)-C(24)-Cl(1)'	106.1 (19)	
F(1a)-B(1)-F(3a)		107.8 (5)	F(5a)-B(2)-F(6a)		105.6 (4)
F(1a)-B(1)-F(4a)		106.8 (4)	F(5a)-B(2)-F(7a)		107.9 (5)
F(2)-B(1)-F(3a)		111.9 (4)	F(5a)-B(2)-F(8a)		109.9 (5)
F(2)-B(1)-F(4a)		109.0 (3)	F(6a)-B(2)-F(7a)		116.2 (6)
F(3a)-B(1)-F(4a)		111.9 (5)	F(6a)-B(2)-F(8a)		108.2 (6)
F(1b)-B(1)-F(2)		117. (1)	F(7a)-B(2)-F(8a)		108.9 (6)
F(1b)-B(1)-F(3b)		114. (2)	F(5b)-B(2)-F(6b)		104.5 (8)
F(1b)-B(1)-F(4b)		106. (1)	F(5b)-B(2)-F(7b)		118.5 (8)
F(2)-B(1)-F(3b)		111. (2)	F(5b)-B(2)-F(8b)		108.3 (5)
F(2)-B(1)-F(4b)		107.8 (6)	F(6b)-B(2)-F(7b)		107.0 (7)
F(3b)-B(1)-F(4b)		100. (1)	F(6b)-B(2)-F(8b)		107.8 (7)
			F(7b)-B(2)-F(8b)		110.0 (9)

[a] The esd's of the least significant digits are given in parameters.

for the ion-paired complex. In the computations actually used, the values of k_a, k_b, k_c, and K_{IP1} were simultaneously corrected to zero ionic strength, as given by the relationship in eq 4. The complete equations are given in the Appendix. In these calculations, the $(\Delta z^2)^{\ddagger}$ terms were held at value of +4, +4, +2, and −4 for k_a, k_b, k_c, and K_{IP1}, respectively.

Least-squares fits to the ionic strength dependence data in Table X by eq 5 resulted in $k^0_{a12} = 1.06 \pm 0.16 \times 10^4$ M^{-1} s^{-1}, where K_{IP1} assumed the value of $2.38 \pm 0.76 \times 10^2$ M^{-1}, and $k^0_{a13} = 1.15 \pm 0.14 \times 10^4$ M^{-1} s^{-1} with $K_{IP1} = 3.11 \pm 0.71 \times 10^2$ M^{-1}. Here the "0" superscript indicates extrapolation in zero ionic strength, as performed by the program. The least-squares fits are shown in Figure 6 (parts A and B). The fact that the calculated association constants are equal to one another, within experimental error, as well as to that determined by the conductivity measurements ($K_{IP1} = 3 \pm 2 \times 10^2$ M^{-1}) supports the legitimacy of this approach.

The possibility that the ion pair is also reactive was investigated by treatment of the same data sets by the more complicated eq 6. With all three parameters floating, the program would not converge, but with K_{IP1} held fixed at the value determined by the conductivity experiments (300 M^{-1}), the values of k_b and k_c in eq 6 took on values of $k^0_{b12} = 7.48 \pm 1.48 \times 10^3$, $k^0_{c12} = 1.21 \pm 0.40 \times 10^4$, $k^0_{b13} = 1.11 \pm 0.19 \times 10^4$, and $k^0_{c13} = 4.23 \pm 50 \times 10^2$ M^{-1} s^{-1}. These fits are comparable in quality to those obtained with eq 5. In the case of reaction 2, the k_c pathway has a large statistical uncertainty, while in the case of reaction 3, the k_c pathway is completely insignificant. Another approach to assessing the importance of the k_c pathway is the experiment in which BPh_4^- is substituted for BF_4^-. This comparison was made by using the observed rate constant $k_{12BPh_4^-} = 4.25$ s^{-1} for the BPh_4^--substituted reaction 2 at $\mu = 9.7$ mM, shown in Table X. The fact that the change of rate was small also suggests that the k_c pathway does not dominate.

A more detailed treatment of the effect of adding BPh_4^- recognizes that K_{IP} and the ion-size parameter should be corrected for the change in electrolyte. It was found that $E_{1/2}$ for $[Cu^{I/II}(py)_2DAP]$ in the two media differed by only 2 mV, indicating a difference in K_{IP} values less than 15 M^{-1}. On the basis of published activity data in BPh_4^- media, the ion-size parameter Ba was increased to 2.53 $M^{-1/2}$.[19] Using eq 5 to extrapolate $k_{a12BPh_4^-}$ to zero ionic strength, with the parameters given, yields $k^0_{a12BPh_4^-} = 1.06 \times 10^4$ M^{-1} s^{-1}, which is identical with the value calculated for the BF_4^- medium. Thus, eq 5 appears to be a thoroughly satisfactory treatment for a change in the identity of the background electrolyte. The evidence supporting a pathway through an ion pair, under the present conditions, is weak, and throughout the remainder of this paper, only the k_a pathway is further considered. Borchardt and Wherland likewise have reported that ion association does not enhance electron-transfer rates for reactions between monocations and neutral species.[23] In the present case, the effect may be considered more surprising because of the significant electrostatic repulsion between the mono- and dications.

Self-Exchange Kinetics. A low-resolution ^1H NMR spectrum of $[Cu^{I}(py)_2DAP]^+$ has previously been published.[8] The high-resolution spectrum shows a weakly coupled triplet ($J = 1.32$ Hz) for the equivalent methyl group protons at 2.27 ppm, a triplet ($J = 6.3$ Hz) for the β-methylene protons at 3.56 ppm, and a triplet for the α-methylene adjacent to the imino nitrogen atom; the latter signal occurs at 4.13 ppm. The aromatic protons at 7.0–8.5 ppm are coupled in a complicated fashion. A ^1H COSY spectrum has been used to establish both the aliphatic and aromatic coupling schemes, verifying that weak coupling occurs between the methyl group protons and the α-methylene protons. No coupling was observed between the central pyridine protons and the methyl

(23) Borchardt, D.; Wherland, S. *Inorg. Chem.* **1986**, *25*, 901–905.

Table VI.

	Cu^{I}	Cu^{II}		Cu^{I}	Cu^{II}
		A. Least-Squares Planes[a]			
		Plane 1: N(3)–C(10)			
A	−0.9772	0.7004	C(7)	0.004	−0.007
B	0.0668	0.5793	C(8)	−0.001	−0.001
C	−0.2015	−0.4168	C(9)	−0.004	0.007
D	11.4871	−2.0684	C(10)	−0.006	−0.007
N(3)	−0.004	−0.001	Cu[b]	−0.079	−0.348
C(6)	−0.002	0.008			
		Plane 2: N(5)–C(15)			
A	0.4861	−0.2549	C(12)	−0.007	0.010
B	−0.7537	−0.7521	C(13)	0.019	−0.005
C	−0.4423	−0.6077	C(14)	−0.019	−0.003
D	−5.7644	3.4804	C(15)	0.007	0.004
N(5)	0.006	0.001	Cu[b]	0.377	0.446
C(11)	−0.005	−0.008			
		Plane 3: DAP^{+}			
A	0.4909	−0.3341	C(16)	−0.032	0.019
B	0.8201	0.5340	C(17)	0.340	−0.115
C	−0.2940	−0.7766	C(18)	−0.057	−0.014
D	−5.7444	0.2498	N(2)	−0.195	0.064
N(1)	0.006	0.027	C(20)	0.066	−0.050
C(1)	−0.053	0.048	C(21)	0.060	−0.023
C(2)	−0.059	0.059	C(22)	−0.008	0.070
C(3)	−0.152	0.028	N(4)	0.047	−0.063
C(4)	0.003	−0.021	Cu[b]	−0.045	−0.012
C(5)	0.033	−0.027			
		Plane 4: DAP			
A	0.5026	−0.3277	C(5)	0.043	−0.030
B	0.8203	0.5315	C(16)	0.055	−0.011
C	−0.2727	−0.7811	C(18)	0.036	−0.047
D	−5.9079	0.2635	N(2)	−0.118	0.038
N(1)	0.039	0.016	C(20)	0.044	−0.043
C(1)	0.014	0.026	C(22)	−0.064	0.086
C(2)	0.013	0.035	N(4)	0.022	−0.057
C(3)	−0.104	0.013	Cu[b]	−0.021	−0.022
C(4)	−0.020	−0.025			
		Plane 5: N(1), N(3), N(5)			
A	−0.1152	0.7514	N(1)	0.000	0.000
B	0.1508	−0.5297	N(2)	0.000	0.000
C	−0.9818	−0.3934	N(3)	0.000	0.000
D	1.5979	1.0206	Cu[b]	−0.021	−0.014

planes	M = Cu^{I}	M = Cu^{II}	M = Cu^{IIc}
	B. Interplanar Angles (deg)		
1–2	64.1	68.8	75.8
1–3	68.5	66.5	54.1
1–4	67.8	66.2	54.1
1–5	71.3	67.4	71.4
2–3	75.5	81.1	77.4
2–4	75.3	80.9	77.5
2–5	74.7	63.5	65.8
3–4	1.4	0.5	0.1
3–5	69.2	76.8	78.3
4–5	70.5	77.3	78.2

[a] The planes are described by the four coefficients of the expression: $Ax + By + Cz + D = 0$. Planes are defined for comparison with ref 11. [b] The position of the metal (Cu) was not included in the calculation of any of the planes. [c] Reference 11 for $[Cu^{II}(imidH)_2DAP]^{2+}$.

protons. The remaining aliphatic and aromatic protons were coupled in a predictable manner.

Dynamic NMR measurements of the $[Cu(py)_2DAP]^{+/2+}$ system were carried out by observing the homonuclear spin-decoupled methyl resonance. The rate constant for electron exchange was obtained from relaxation times according to

$$1/T_2 = 1/T_{2e} + 1/T_{2n} = k'_{11}[Cu^{II}(py)_2DAP] + 1/T_{2n} \quad (7)$$

which is applicable in the slow-exchange regime.[19] In this equation, $1/T_{2e}$ is the contribution to the transverse relaxation time due to the chemical exchange, while $1/T_{2n}$ is the natural transverse relaxation time in the absence of chemical exchange. Values of $1/T_2$ were obtained both by the Carr–Purcell–Mieboom–Gill method as well as by the line-broadening method. In the latter method, $1/T_2 = \pi\Delta\nu_{1/2}$, where $\Delta\nu_{1/2}$ is equal to the FWHM of the NMR resonance. Since the NMR spectrum of $[Cu^{II}(py)_2DAP]^{2+}$ is unobservable because of extensive paramagnetic broadening, the spectra of the mixed samples show the resonances of the copper(I) species only. Values of $1/T_2$ are listed in Table XI, and a plot of $1/T_2$ vs. the concentration of added $[Cu^{II}(py)_2DAP]^{2+}$ is illustrated in Figure 7. The linear relationship affords k'_{11} as the slope and $1/T_{2n}$ as the intercept. The resulting experimental value for k'_{11} is $1.7 \pm 0.2 \times 10^3$ M^{-1} s^{-1} at $\mu = 0.05$ M and $T = 27$ °C.

The first-order dependence of the apparent rate constant for electron self exchange, k_{11obsd}, upon the concentration of the

Table VII. Comparison of the Various Cu–N Distances (Å) in $[Cu^{I}(py)_2DAP]^{+}$, $[Cu^{II}(py)_2DAP]^{2+}$, and $[Cu^{II}(imidH)_2DAP]^{2+}$

nitrogen atom	Cu^{I}	Cu^{II}	$Cu^{II}(imidH)_2DAP$
central pyridine	2.094	1.920	1.923
terminal rings	2.032	2.033	1.992
	2.083	2.129	2.081
imino[a]	2.256	2.018	2.051
all[b]	2.144	2.024	2.020

[a] The average of two values. [b] The average of five values.

Table VIII. Formal Potentials of the Copper Complexes and Calculated Equilibrium Quotients at $\mu = 38$ mM in CH_3CN[a]

complex	ΔE_p, mV[b]	$E_{1/2}$, V[b]	$E_{1/2}$, V[c,d]	FWHM, mV[c]	E'', V[e]
$[Cu(py)_2DAP]^{n+}$	78	−0.136	−0.154	96	−0.116
$[Cu(imidH)_2DAP]^{n+}$	76	−0.269	−0.284	100	−0.261
$[Cu(imidR)_2DAP]^{n+}$	76	−0.256	−0.251	96	−0.246

$[Cu^{II}(py)_2DAP]^{2+}$ reductant	ΔE, V[b]	$\Delta E''$, V[e]	K[f]	K''[g]
$[Cu^{I}(imidH)_2DAP]^{+}$	0.133	0.145	177	283
$[Cu^{I}(imidR)_2DAP]^{+}$	0.120	0.130	107	158

[a] Complexes at 1.0 mM, ionic strength medium n-Bu_4NBF_4 in CH_3CN, all potentials vs. SCE, recorded at Pt button electrode. Ion pairing correction to $[n\text{-}Bu_4NBF_4] = 47$ mM gives $\mu = 0.038$ M. [b] By cyclic voltammetry, scan rate = 20 mV s^{-1}. [c] By differential pulse voltammetry, shifted by IR drop. [d] $E_{1/2} = E_{max} + E_{ma/2}$; E_{ma} = modulation amplitude = 50 mV. [e] $E_{1/2}$ from CV experiment corrected for ion pairing contributions. $K_{IP1} = 300$ M^{-1}, $K_{IP2} = 100$ M^{-1}, K_{IP3} assumed = 100 M^{-1}. [f] $\ln K = \Delta EnF/RT$. [g] $\ln K'' = \Delta E''nF/RT$.

Table IX. Observed Rate Dependence on Concentrations of Reactants in Cross-Exchange Reactions[a]

A. $[Cu^{II}(py)_2DAP]^{2+} + [Cu^{I}(imidH)_2DAP]^{+}$[b]

$[[Cu^{II}(py)_2DAP]^{2+}]$, mM	k_{12obsd}, s^{-1}[c]	$[[Cu^{II}(py)_2DAP]^{2+}]$, mM	k_{12obsd}, s^{-1}[c]
0.1	2.53	0.7	15.5
0.2	4.79	0.8	18.7
0.3	7.45	0.9	21.6
0.4	9.66	1.0	24.4
0.5	12.9	0.2[d]	4.84
0.6	14.5	0.2[e,f]	4.42

B. $[Cu^{II}(py)_2DAP]^{2+} + [Cu^{I}(imidR)_2DAP]^{+}$[g]

$[[Cu^{II}(py)_2DAP]^{2+}]$, mM	k_{13obsd}, s^{-1}[c]	$[[Cu^{II}(py)_2DAP]^{2+}]$, mM	k_{13obsd}, s^{-1}[c]
0.1[f]	2.68	0.6	11.39
0.2	4.64	0.8	15.10
0.4	6.26	1.0	17.57

[a] In CH_3CN at 25.0 °C and $\mu = 0.01$ M (n-Bu_4NBF_4), ion pairing constant of electrolyte $K = 10$ M^{-1} (ref 17) gives effective $\mu = 9.0$ mM. [b] $[Cu^{I}(imidH)_2DAP]^{+}_0 = 1 \times 10^{-5}$ M. [c] k_{obsd} values are averages of ~3 separate experients, each of which was performed with signal averaging for ~6 shots. [d] $[Cu^{I}(imidH)_2DAP]^{+}_0 = 5 \times 10^{-6}$ M. [e] $[Cu^{I}(imidH)_2DAP]^{+}_0 = 4 \times 10^{-5}$ M. [f] Major species is in only 5× excess. [g] $[Cu^{I}(imidR)_2DAP]^{+}_0 = 2 \times 10^{-5}$ M.

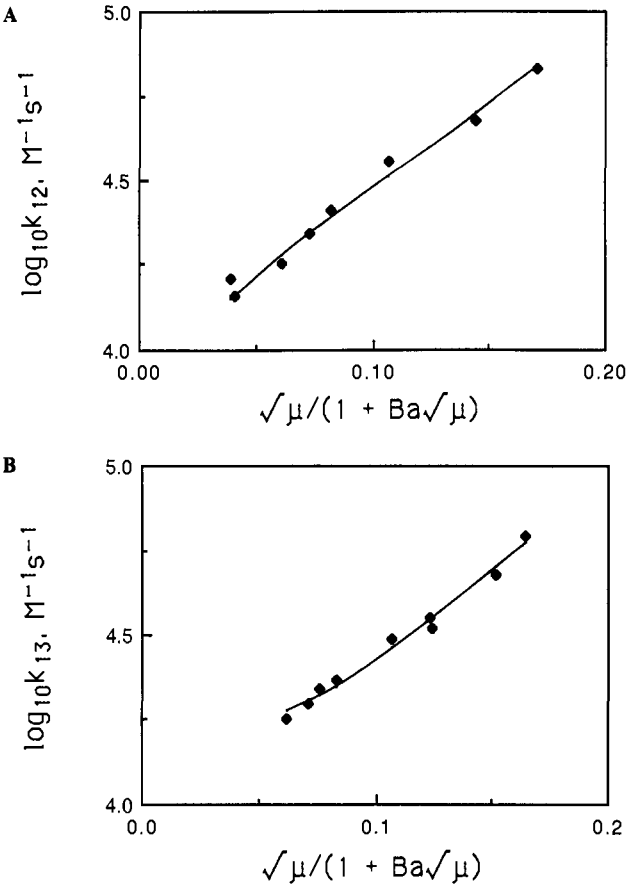

Figure 6. Ionic strength dependence of the second-order electron-transfer rate constants: A, eq 2; B, eq 3 (see text). Experimental results are the solid diamonds; the solid line is the fitted function of eq 5 holding K_{IP1} = 300 M^{-1}. Reactant concentrations were held at [Cu(II)] = 0.2 mM and [Cu(I)] = 0.02 mM. Both reactions at 25.0 °C in CH_3CN with n-Bu_4NBF_4 as the background electrolyte.

Table X. Kinetic Medium Effects for Cross Reactions

A. $[Cu^{I}(imidH)_2DAP]^+ + [Cu^{II}(py)_2DAP]^{2+}$ [a]

μ, mM[b]	k_{obsd12}, s^{-1}	μ, mM[b]	k_{obsd12}, s^{-1}
1.8	3.22	17	7.18
2.0	2.87	37	9.63
4.6	3.52	52	13.5
6.8	4.33	9.7[c]	4.25
9.0	4.91		

B. $[Cu^{I}(imidR)_2DAP]^+ + [Cu^{II}(py)_2DAP]^{2+}$ [d]

μ, mM[b]	k_{obsd13}, s^{-1}	μ, mM[b]	k_{obsd13}, s^{-1}
4.8	3.62	17	6.06
6.6	4.03	25	6.91
7.5	4.36	42	9.55
9.3	4.64	52	12.2

[a] In CH_3CN at 25 °C. $[[Cu^{I}(imidH)_2DAP]^+]_0$ = 1 × 10^{-5} M, $[[Cu^{II}(py)_2DAP]^{2+}]$ = 0.2 mM. [b] Corrected for ion pairing of n-Bu_4NBF_4, K_{IP} = 10 M^{-1}.[17] [c] Medium maintained with $NaBPh_4$, [n-Bu_4NBF_4] = 0.3 mM, ion pairing constant[36] of $NaBPh_4$ K = 4 M^{-1} gives effective μ = 9.7 mM. [d] In CH_3CN at 25 °C. $[[Cu^{I}(imidR)_2DAP]^+]_0$ = 2 × 10^{-5} M, $[[Cu^{II}(py)_2DAP]^{2+}]$ = 0.02 mM.

spectroscopically unobservable copper(II) species is the only kinetic information derivable from these NMR experiments. The required high concentration of both the copper(I) complex and the supporting electrolyte precluded lowering their values, and the limiting solubility of the electrolyte prevented the use of higher concentrations. Thus, experiments to measure the ionic strength dependence and the proposed copper(I) concentration independence of T_2 were not practical. However, it is reasonable to assume that the detailed rate law is the same as for the cross reactions studied above, in greater detail, by the stopped-flow method.

Table XI. $1/T_2$ Variation with Copper(II) Concentration[a]

$[Cu^{II}]$, mM	$1/T_2$, Hz (by $\Delta\nu_{1/2}$)	$1/T_2$, Hz (CPMG)	$1/T_2$, Hz (mean)
0.0	1.41	1.34	1.38
0.5	1.72	1.47	1.60
1.5	3.96	4.11	4.03
3.0	6.30	8.61	7.46
4.0	8.80	9.15	8.98
5.0	10.68		10.68
5.2	8.55	8.33	8.64

[a] Least-squares slope = (1.76 ± 0.16) × 10^3 M^{-1} s^{-1}; μ = 0.05 M (Me_4NBF_4); $[Cu^{I}(py)_2DAP]^+$ held at 5 mM; T = 27 °C.

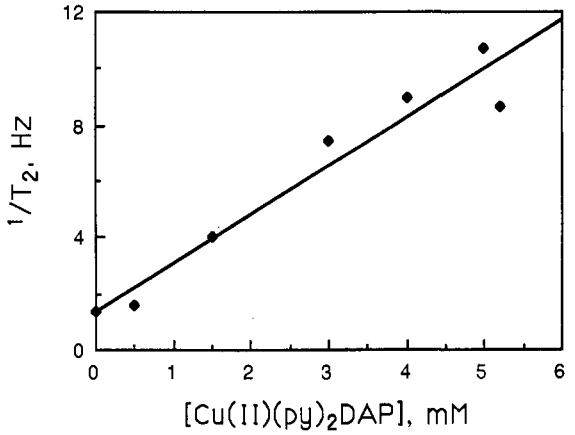

Figure 7. Dependence of longitudinal relaxation time of $[Cu^{I}(py)_2DAP]^+$ homonuclear spin-decoupled methyl ^1H resonance upon the concentration of $[Cu^{II}(py)_2DAP]^{2+}$ in solution. Copper(I) concentration was held at 5 mM in CD_3CN and ionic strength, μ = 0.05 M (Me_4NBF_4). Plotted valued are averages of values obtained by the line width and the Carr–Purcell–Mieboom–Gill methods. The measurements were made at T = 27 °C with samples sealed under inert atmosphere.

Discussion

Solid-State Structural Comparisons. The present case is among the few well-documented examples of copper complexes in both 1+ and 2+ oxidation states having common pentacoordinate ligand environments.[24,25] Moreover, the fixed pentacoordinate geometry that this system displays is rare even when all transition metals are considered. To our knowledge, the only other copper system with these characteristics is that reported by Nelson,[26,27] which employs metal ligation by sulfur and nitrogen within a ligand similar to $(py)_2DAP$, but which has a cyclic thioether moiety substituted for the two alkylpyridine groups. Both of the present complexes possess a unique pyridine nitrogen donor atom and two imino nitrogen donor atoms (derived from 2,6-diacetylpyridine (DAP)) as well as two terminal pyridine group donor atoms from the alkylpyridines (py). Moreover, the crystal structure of $[Cu^{II}(imidH)_2DAP](BF_4)_2$ has been previously reported,[11] and the comparison of these three related structures seems warranted.

The $(imidH)_2DAP$ ligand is similar to $(py)_2DAP$, with imidazole moieties replacing the two terminal pyridine rings. In general, the two different pentadentate ligands envelope the metal ions in the same fashion, regardless of oxidation state. However, as discussed below, the details of the coordination polyhedra for the 1+ and 2+ oxidation states are best described in somewhat different terms. The difference in the average Cu–N bond distances between the two complexes, $[Cu^{I}(py)_2DAP]^+$ and $[Cu^{II}(imidH)_2DAP]^{2+}$, is 0.12 Å. However, these distance changes occur in a quite asymmetric fashion. Moreover, a comparison of the dihedral angles between equivalent planes in the two

(24) Dagdigian, J. V.; McKee, V.; Reed, C. A. *Inorg. Chem.* **1982**, *21*, 1881–1886.
(25) Burke, P. J.; Henrick, K.; McMillin, D. R. *Inorg. Chem.* **1982**, *21*, 1332–1342.
(26) Drew, M. G. B.; Cairns, C.; McFall, S. G.; Nelson, S. M. *J. Chem. Soc., Dalton Trans.* **1980**, 2020–2027.
(27) Drew, M. G. B.; Cairns, C.; Nelson, S. M.; Nelson, J. *J. Chem. Soc., Dalton Trans.* **1981**, 942–948.

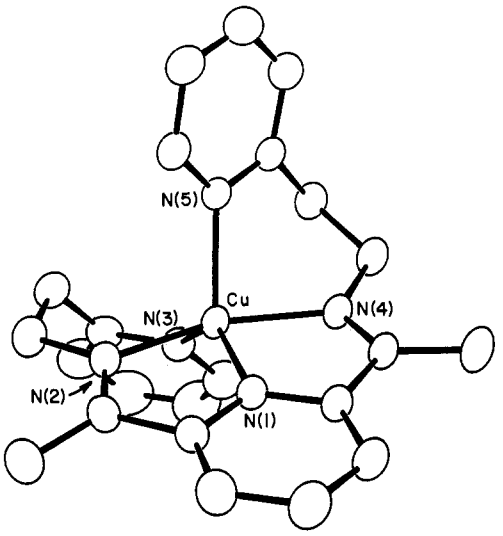

Figure 8. A computer-drawn view of the $[Cu^{II}(py)_2DAP]^{2+}$ cation designed to show the quasi-square-pyramidal coordination geometry around the copper(II) metal center.

complexes, given in Table VI, shows that there are genuine differences in the detailed conformation of the two complexes. Thus, the differences in Cu–N bond distances could result from a combination of the differing pendant groups (conformation effects) and the changes in oxidation state. Interestingly, the deviation from an idealized trigonal bipyramid in isoelectronic $[Zn^{II}(imidH)_2DAP]^{2+}$ is much larger than in $[Cu^{I}(py)_2DAP]^{+}$, again suggesting the possible importance of ligand effects on the metal–ligand bond distances of the complex.

In order to compare more accurately the differences in the copper(I) and copper(II) structures resulting solely from oxidation state changes, a variety of attempts to prepare crystalline Cu(I) and Cu(II) complexes utilizing the same pentadentate ligand was commenced. These eventually led to the preparation of crystalline $[Cu^{II}(py)_2DAP](BF_4)_2$. An important question about the $[Cu^{II}(py)_2DAP]^{2+}$ ion is how best to describe the coordination polyhedron around the central copper(II) ion. As shown in Figure 8, the general trigonal bipyramidal description used for the copper(I) analogue is no longer as valid. Indeed, although the "axial" N(2)CuN(4) angle has increased to 158.27 (9)°, and the three atoms N(1), N(3), and N(5) define a plane which again contains the Cu(II) ion (within 0.01 Å), the NCuN angles in this trigonal plane are quite unequal: N(3)CuN(5) = 106.4 (9)° while N(1)CuN(3) = 134.42 (8)° and N(1)CuN(5) = 119.53 (8)°. These angles suggest that the alternative description of a square pyramidal complex with the N(5) pyridine as the axial ligand is more suitable for the present case. In this view, the copper(II) ion is displaced 0.45 Å from the mean plane defined by the other four nitrogen donor atoms. A similar square pyramidal description of the coordination group for the $[Cu^{II}(imidH)_2DAP]^{2+}$ ion also seems equally valid.[28] An immediate virtue of this description for the coordination polyhedron is an explanation for the one long[29] Cu–N distance in both copper(II) complexes where this Cu–N bond would correspond to the axial (z) direction in a complex having the $d_{x^2-y^2}$ orbital only singly populated.

The average difference in the Cu–N distances of $[Cu^{I}(py)_2DAP]^{+}$ and $[Cu^{II}(py)_2DAP]^{2+}$ has the same asymmetric pattern noted earlier for $[Cu^{I}(py)_2DAP]^{+}$ and $[Cu^{II}(imidH)_2DAP]^{2+}$. The average bond distances to the two terminal pyridine ring nitrogens differ by only 0.02 Å, with the copper(I) complex actually having the shorter bonds[30] (average values are 2.081 (68) Å in the Cu(II) species and 2.058 (36) Å in the Cu(I) complex.) The bond to the central pyridine nitrogen donor atom differs by 0.17 Å, while the difference between the imino nitrogen donor atoms is larger still at 0.24 Å (2.018 (12) Å for Cu(II) vs. 2.256 (23) Å for Cu(I)).[31] Values for the various types of Cu–N bond distances in the three complexes are given in Table VII. The values in the table clearly show the great similarity in bond distances for $[Cu^{II}(py)_2DAP]^{2+}$ and $[Cu^{II}(imidH)_2DAP]^{2+}$. Therefore, we conclude that the difference between bond distances in $[Cu^{I}(py)_2DAP]^{+}$ and $[Cu^{II}(py)_2DAP]^{2+}$ and the asymmetry in the differences for the various donor atom types are primarily the result of the oxidation state change.

Calculated least-square planes for $[Cu^{II}(py)_2DAP]^{2+}$ are given in Table VI. Conformational aspects of this complex are shown at the end of Table VI which details the interplanar angles noted previously. Again, there are conformational differences between the copper(I) and copper(II) complexes. The comparison of the interplanar angles for the three complexes suggests that the conformational differences result from the combination of bond distance changes and pendant group changes.

A general characteristic of redox-active copper complexes utilizing the same ligand system has been the increase in coordination number of the copper(II) derivative compared to that of the copper(I) case.[24,25,32] That this does not occur with the present system is a consequence of the steric constraints imposed by the pentadentate $(py)_2DAP$ ligand. In fact, the present $[Cu^{I}(py)_2DAP]^{+}$ cation represents only the third well-characterized example of pentacoordinate copper(I) known to us.[26,33] On the other hand, four- and even three-coordinate (often T-shaped)[24,34] geometries appear to be more normal for copper in the 1+ oxidation state.

Since the solution phase chemistry of these complexes is subject to relatively large ion-pairing constants,[17,35] it was instructive to examine the unit cell packing interactions to inspect for any specific ion–ion interactions. The copper(I) compound crystal structure shows no close contacts between the BF_4^- anion and the copper(I) complex, but short inter-atomic distances between one BF_4^- ion and the copper–imino nitrogen region of the cation in the $[Cu^{II}(py)_2DAP](BF_4)_2$ salt do seem to occur, which suggests a specific site for ion pairing in solution. These key bond distances are as follows: Cu–F, 3.67 Å; Cu–F, 3.44 Å; N_2–F, 3.11 Å; and C_{16}–F, 2.97 Å.

Solution-State Chemistry. From the crystallographic studies, $[Cu^{II}(py)_2DAP]^{2+}$, $[Cu^{II}(imidH)_2DAP]^{2+}$, and $[Cu^{I}(py)_2DAP]^{+}$ are all pentacoordinate and have similar structures. It is reasonable to assume that the remaining copper complexes investigated in this paper also have similar solid-state structures, but a question still arises as to their structures in solution. Copper K-edge

(28) In the copper(II) structures, the two terminal ligands are distinct, and only one possible choice of square-pyramidal axial ligand is appropriate. In the copper(I) structure, the N(5) or the N(3) pyridine ring can equally well be chosen as the axial group. The copper(I) is displaced by 0.63 or 0.61 Å from the two possible choices of basal plane. In $[Cu^{II}(py)_2DAP]^{2+}$, the copper(II) ion is displaced 0.61 Å from the alternate choice of basal plane. In $[Cu^{II}(imidH)_2DAP]^{2+}$, the copper(II) displacements are 0.42 and 0.62 Å from the two possible basal planes, with smaller displacement than from the better basal plane.

(29) In $[Cu^{II}(py)_2DAP]^{2+}$, Cu–N(5) = 2.129 (2) Å and in $[Cu^{II}(imidH)_2DAP]^{2+}$, Cu–N = 2.081 (6) Å.

(30) This is in distinct contrast to the usual expectation that all bond lengths in the complex with the lower metal oxidation state will be longer. In the present case, the comparison is clouded by the changes in the nature of the coordination polyhedron and the accompanying differences in the metal–ligand bonds.

(31) The numbers in parentheses are the variances in the averaged bond distances.

(32) (a) Brubaker, G. R.; Brown, J. N.; Yoo, M. K.; Kinsey, R. A.; Kutchan, T. M.; Mottel, E. A. *Inorg. Chem.* **1979**, *18*, 299–302. (b) Corfield, P. W. R.; Cecarelli, C.; Glick, M. D.; Moy, I. W.; Ochrymowycz, L. A.; Rorabacher, D. B. *J. Am. Chem. Soc.* **1985**, *107*, 2399–2404. (c) Diaddario, L. L., Jr.; Dockal, E. R.; Glick, M. D.; Ochrymowycz, L. A.; Rorabacher, D. B. *Inorg. Chem.* **1985**, *24*, 356–363.

(33) Gagne, R. R.; Allison, J. L.; Gall, R. S.; Koval, C. A. *J. Am. Chem. Soc.* **1977**, *99*, 7170–7178.

(34) (a) Sorrell, T. N.; Malachowcki, M. R.; Jameson, D. L. *Inorg. Chem.* **1983**, *21*, 3250–3252. (b) Sorrell, T. N.; Malachowski, M. R. *Inorg. Chem.* **1983**, *22*, 1883–1887.

(35) (a) Braga, T. G.; Wahl, A. C. *J. Phys. Chem.* **1985**, *89*, 5822. For PF_6^- and BF_4^- salts of $[Fe(bpy)_3]^{2+}$ and similar complexes association constants are less than 50 M^{-1}. (b) Diamond, A.; Fanelli, A.; Petrucci, S. *Inorg. Chem.* **1973**, *12*, 611–619. Association constants of 42–75 M^{-1} for ClO_4^- salts of Ni^{2+}, Zn^{2+}, Cu^{2+}. (c) Libus, W.; Chachulski, B.; Fraczyk, L. *J. Sol. Chem.* **1980**, *9*, 355–369. Association constants of 107–150 M^{-1} for BF_4^- salts of Mn^{2+}, Co^{2+}, Ni^{2+}, Cu^{2+}, and Zn^{2+}.

Table XII. Rate Constants for Electron Transfer at 25 °C in CH_3CN for the Three Copper Complexes

	k', M^{-1} s^{-1}, μ = 50 mM	k'', M^{-1} s^{-1}, μ = 38 mM	k^0, M^{-1} s^{-1}, μ = 0.0 mM
k_{11}	1.7×10^3 [a]	2.8×10^3 [d]	3.0×10^2 [e]
k_{22}	1.7×10^4 [b]	1.5×10^4 [f]	1.6×10^3 [g]
k_{33}	2.4×10^4 [b]	3.1×10^4 [f]	3.4×10^3 [g]
k_{12}	6.4×10^4 [c]	9.8×10^4 [d]	1.1×10^4 [h]
k_{13}	6.1×10^4 [c]	1.1×10^5 [d]	1.2×10^4 [h]

[a] From NMR study at μ = 50 mM. [b] Calculated with eq 8 and 9; K_{12} = 178 and K_{13} = 107 measured at μ = 38 mM. [c] From cross-exchaange measurement at μ = 52 mM. [d] k^0, corrected to μ = 38 mM by eq 4 where $(\Delta z^2)^\ddagger$ = 4, Ba = 1.70. [e] k'_{11} extrapolated to μ = 0.0 mM by eq 5. [f] Uses K'' values in Table VIII. [g] Extrapolated to μ = 0.0 mM by using eq 4, with $(\Delta z^2)^\ddagger$ = 4, Ba = 1.70. [h] Derived from least-squares fit of eq 5 to ionic strength dependent k_{obsd}.

EXAFS results reported previously for the imidazole derivative in its Cu(I) and Cu(II) states imply that pentacoordination is retained in solution.[10] In addition, NMR results obtained in this work for the three Cu(I) derivatives demonstrate that the ligands retain their integrity in solution and that the two halves of each ligand are equivalent. This stands in contrast with the crystallographic results, where the two halves of the ligand, although similar, differ in detail and prevent assigning C_2 symmetry. Apparently, there is subtle fluxionality in solution that leads to NMR equivalence. Overall, it seems quite probable that the predominant species in solution have pentacoordinate structures rather similar to those determined for the solid state.

The rate laws for electron transfer between these pentacoordinate Cu(I) and Cu(II) complexes imply a simple bimolecular mechanism. A simple inner-sphere mechanism is unlikely because the ligands do not provide any lone pairs for bridging. However, it is conceivable that an arm of one ligand could dissociate from its Cu(I) center, rotate, bind to an adjacent Cu(II) center, and thus form a bridge for an inner-sphere mechanism. Substitution rates are unknown for these complexes, but the high lability generally ascribed to Cu(I) is consistent with this mechanism. On the other hand, it is not clear that such an inner-sphere mechanism would confer any advantages relative to a simple outer-sphere mechanism. Furthermore, an outer-sphere mechanism might be anticipated because of the small structural differences between the two oxidation states and the ample opportunity for adiabatic overlap. If such is the case, then Marcus theory can be applied.

Treatment of the current set of rate constants may be carried out with the well-known Marcus cross relation

$$k_{12} = (k_{11}k_{22}K_{12}f_{12})^{1/2} \quad (8)$$

where

$$\ln f_{12} = (\ln K_{12})^2/4 \ln (k_{11}k_{22}/Z^2) \quad (9)$$

is used to estimate values for the self-exchange rate constants k_{22} ($[Cu^{I,II}(imidH)_2DAP]^{n+}$) and k_{33} ($[Cu^{I,II}(imidR)_2DAP]^{n+}$). As a first approximation, these calculations were performed without regard to ionic strength dependences of the rate constants or equilibrium quotients or to ion-pairing effects in the rate laws, because these effects may be expected largely to cancel. The values used in these calculations were simply the experimental results listed in Table XII. The f term in eq 9 required initial estimates for k_{22} and k_{33}. These were obtained by assuming $k_{11} = k_{22} = k_{33}$. The final values of k_{22} and k_{33} calculated through eq 8 and 9 are also listed in Table XII as $k'_{22} = 1.7 \times 10^4$ M^{-1} s^{-1} and $k'_{33} = 2.4 \times 10^4$ M^{-1} s^{-1}. These two self-exchange rate constants are roughly an order of magnitude larger than the directly measured k'_{11} value.

A more detailed analysis that accounts for the effects of ion association and activity coefficients has also been carried out. Experimental rate constants were corrected for ion association as follows. The least-squares fitted parameters k^0_a for both cross reactions were extrapolated to μ = 0.038 M by using eq 4; the resulting values of k''_{12} and k''_{13} are listed in Table XII. The measured self-exchange rate constant, k'_{11}, was first extrapolated to zero ionic strength by eq 5, by using the value of $K_{IP1} = 300$ M^{-1}. The resulting rate constant, listed in Table XII as k^0_{11}, is 3.0×10^2 M^{-1} s^{-1}. Correction of k^0_{11} to μ = 0.038 M by eq 4 yields the value $k''_{11} = 2.8 \times 10^3$ M^{-1} s^{-1}, which is the rate constant for the nonassociated species.

Equilibrium quotients, determined from $E_{1/2}$ measurements, were corrected for ion association by the following procedure. By using the measured K_{IP1} value of 300 M^{-1}, the value of $E_{1/2}$ for $[Cu^{I/II}(py)_2DAP]$ was corrected to give a non-ion-paired reduction potential $E''_1 = -0.136 - (0.020) = -0.116$ V vs. SCE. Using the moderately large value of $K_{IP2} = 100$ M^{-1}, as determined by conductivity, and assuming that K_{IP3} is of similar magnitude allows correction of E_2 and E_3 to $E''_2 = -0.261$ V and $E''_3 = -0.246$ V vs. SCE. The $\Delta E''_{12}$ and $\Delta E''_{13}$ values shown in Table VIII result in $K''_{12} = 283$ M^{-1} and $K''_{13} = 158$ M^{-1}. The superscript "″" indicates the correction for ion pairing at μ = 0.038 M.

Applying the cross relationship to k''_{11}, k''_{12}, k''_{13}, K''_{12}, and K''_{13} gives $k''_{22} = 1.5 \times 10^4$, and $k''_{33} = 3.1 \times 10^4$. These values, when corrected to zero ionic strength by eq 4, give $k^0_{22} = 1.6 \times 10^3$ and $k^0_{33} = 3.4 \times 10^3$, all in M^{-1} s^{-1}. By comparing values of the self-exchange rate constants, k'_{nn} and k''_{nn}, shown in Table XII, it is apparent that the effects of ion pairing do not significantly affect the results from the cross relationship.

On the basis of steric effects on the solvent reorganizational energy, one would expect the self-exchange rate for $[Cu(imidR)_2DAP]^{2+/+}$ to be substantially greater than for the other complexes. Such is the case for $[Cu(py)_2DAP]^{2+/+}$. We have no simple explanation for the fivefold greater rate of $[Cu(imidH)_2DAP]^{2+/+}$ over $[Cu(py)_2DAP]^{2+/+}$, but the difference may simply reflect the combined effects of experimental error and approximations implicit in the cross relationship. The general success of the cross relationship in correlating these rate constants is taken as evidence that the mechanism is outer-sphere, although one should bear in mind Gould's cautions regarding such deductions.[37]

Another approach to assigning the mechanism is to consider whether the magnitude of the rate constants is consistent with outer-sphere electron transfer. For octahedral complexes this is a relatively feasible method, because there is a wealth of unambiguously outer-sphere results for comparison. We know of only one published study of an unambiguously outer-sphere electron-transfer reaction of a pentacoordinate complex and that is the reduction of $[Fe^{III}L(H_2O)]$ by $[Ru^{II}(NH_3)_6]^{2+}$ (L = tetrakis(4-*N*-methylpyridyl)porphine).[38] That study led to an estimate of 1.2×10^6 M^{-1} s^{-1} for the self-exchange rate constant of the Fe^{II}/Fe^{III} couple. Because of the porphyrin ligand rigidity, the bulk of the complex, and the aqueous solvent, $[Fe^{III}L(H_2O)]$, as observed, is expected to have a significantly greater self-exchange rate constant than the present copper complexes. It is difficult to carry out a detailed analysis in terms of internal and solvent reorganizational energies because the force field for these complexes is unknown. At a qualitative level, the Cu^I–N bonds should be rather weak, so there should be only a small internal reorganizational barrier. In conclusion, the self-exchange rates presented in Table XII appear to be consistent with an outer-sphere mechanism of electron transfer.

To our knowledge, there have been no prior published examples of electron transfer for pentacoordinate copper complexes. Pulliam and McMillan have recently reviewed self-exchange reactions for $Cu^{+/2+}$ systems,[7c] but in all cases where data are available there appears to be an accompanying change in coordination number when the Cu(I) and Cu(II) complexes are synthetically derived species. Plastocyanin, a copper redox protein with a tetracoordinate active site, retains its coordination number in both oxidation states for the high-pH form of the protein, whereas there is a tendency toward tricoordinate copper(I) in a low-pH form.[2] In contrast, the active site of azurin, a related blue copper protein,

(36) Yeager, H. C.; Kratochvil, B. *Can. J. Chem.* **1975**, *53*, 3448–3451.
(37) Gould, E. S. *Inorg. Chem.* **1979**, *18*, 900–901.
(38) Pasternack, R. F.; Spiro, E. G. *J. Am. Chem. Soc.* **1978**, *100*, 968–972.

has a quasi-tricoordinate or quasi-pentacoordinate structure for copper(II),[3] depending on one's point of view. For the quasi-pentacoordinate option, the present investigation may, in time, hold additional significance. In any event, self-exchange rate measurements for redox active cuproproteins are heavily influenced by environmental and electrostatic factors,[4,5] and there is hope that well-defined Cu(I)/Cu(II) systems such as those reported here will contribute to a more indepth understanding of the redox and coordination chemistry of the naturally occurring active sites. For the blue copper proteins, this will be especially true if three-, four-, and five-coordinate Cu(I)/Cu(II) pairs can be systematically designed, synthesized, and studied where the coordination number is invariant during redox chemistry and where an outer-sphere mechanism is virtually assured.

Acknowledgment. We thank the National Institutes of Health (Grant HL-15627 to W.R.S. and GM-28451 to L.J.W.), the Robert A. Welch Foundation (Grant C-627 to L.J.W. and Grant C-846 to D.M.S.), and the National Science Foundation (Grant CHE-8215501 to D.M.S.) for support of this research. Discussions with Norman Sutin, Tom Meyer, Scot Wherland, and David McMillin were helpful in preparation of this manuscript. Dr. Alan Kook provided valuable assistance in performing the NMR experiments.

Appendix

The complete equations used for calculations in eq 5 and 6 are given in eq A1 and A2, respectively

$$k_{obsd} = \frac{[Cu^{II}]k_a(\exp(4A\mu^{1/2}/(1 + Ba\mu^{1/2})))}{(1 + K_{IP}[BF_4^-](\exp(-4A\mu^{1/2}/(1 + Ba\mu^{1/2}))))} \quad \text{(A1)}$$

$$k_{obsd} = [Cu^{II}]\{k_a(\exp(4A\mu^{1/2}/(1 + Ba\mu^{1/2}))) + k_bK_{IP}[BF_4^-](\exp(-2A\mu^{1/2}/(1 + Ba\mu^{1/2})))\}/(1 + K_{IP}[BF_4^-](\exp(-4A\mu^{1/2}/(1 + Ba\mu^{1/2})))) \quad \text{(A2)}$$

Supplementary Material Available: Table IS, thermal parameters, Table IIS, fractional coordinates for the fixed atoms for $[Cu^I(py)_2DAP]^+$, Table IIIS, thermal parameters, and Table IVS, calculated hydrogen atom positions, for $[Cu^{II}(py)_2DAP]^{2+}$ (4 pages); listings of observed and calculated structure amplitudes (×10) for $[Cu^I(py)_2DAP]^+$ and $[Cu^{II}(py)_2DAP]^{2+}$ (25 pages). Ordering information is given on any current masthead page.

Where Are the Protons in $H_3V_{10}O_{28}^{3-}$?[1]

V. W. Day,*[2a] W. G. Klemperer,*[2b] and D. J. Maltbie[2b]

Contribution from Crystalytics Company, Lincoln, Nebraska 68501, and the Department of Chemistry, University of Illinois, Urbana, Illinois 61801. *Received August 25, 1986*

Abstract: The protonation sites in $H_3V_{10}O_{28}^{3-}$ have been characterized in the solid state and solution with use of single crystal X-ray diffraction, vapor pressure osmometery, and multinuclear solution NMR techniques. Crystalline $H_3V_{10}O_{28}[(C_6H_5)_4P]_3\cdot 4CH_3CN$ [a = 15.898 (2) Å, b = 16.742 (2) Å, c = 23.646 (4) Å, α = 104.74 (1)°, β = 121.13 (1)°, γ = 108.57 (1)°, Z = 2, space group $P\bar{1}$—C_i^1] contains $H_3V_{10}O_{28}^{3-}$ ions in which three colinear oxygens are protonated, specifically, two OV_2 (doubly bridging) plus one OV_3 (triply bridging) oxygens. These $H_3V_{10}O_{28}^{3-}$ anions are linked together in pairs across a crystallographic inversion center by six hydrogen bonds to form $(H_3V_{10}O_{28})_2^{6-}$ dimers. In 1:4 (v/v) $CH_3CN/CHCl_3$, the $H_3V_{10}O_{28}^{3-}$ ions in $H_3V_{10}O_{28}[(n\text{-}C_4H_9)_4N]_3$ also form dimers. In 1:1 CH_3CN/H_2O solutions of $H_3V_{10}O_{28}[(n\text{-}C_4H_9)_4N]_3$, however, the $H_3V_{10}O_{28}^{3-}$ ion is monomeric. Oxygen-17 NMR spectroscopy identifies two OV_2 and one OV_3 oxygens as the $H_3V_{10}O_{28}^{3-}$ protonation sites in CH_3CN/H_2O solutions of $H_3V_{10}O_{28}[(n\text{-}C_4H_9)_4N]_3$.

A large number of early transition metal polyoxoanion derivatives have been synthesized that incorporate inorganic, organometallic, or organic groups bound to one,[3-10] two,[11] three,[12-17] or five[18] of the six approximately coplanar, closest-packed oxygens that form the faces of hexametallate ($M_6O_{19}^{n-}$) and Keggin ($XM_{12}O_{40}^{n-}$) anions (see **a**). Since steric factors are known to influence binding site preferences in this very simple array,[15,19]

(1) ^{17}O Nuclear Magnetic Resonance Spectroscopy of Polyoxometalates. 4.

(2) (a) Crystalytics Company. (b) University of Illinois.

(3) $HNb_6O_{19}^{7-}$: Lindqvist, I. *Ark. Kemi* **1953**, *5*, 247.

(4) $HV_2W_4O_{19}^{3-}$: (a) Flynn, C. M., Jr.; Pope, M. T. *Inorg. Chem.* **1971**, *10*, 2524. (b) Klemperer, W. G.; Shum, W. *J. Am. Chem. Soc.* **1978**, *100*, 4891.

(5) $PM_{12}O_{40}R$, M = Mo, W and R = CH_3 and/or C_2H_5: Knoth, W. H.; Harlow, R. L. *J. Am. Chem. Soc.* **1981**, *103*, 4265.

(6) $PTiW_{11}O_{40}CH_3^{4-}$: Knoth, W. H.; Domaille, P. J.; Roe, D. C. *Inorg. Chem.* **1983**, *22*, 198.

(7) $H_2PTi_2W_{10}O_{40}^{5-}$: Domaille, P. J.; Knoth, W. H. *Inorg. Chem.* **1983**, *22*, 818.

(8) $[(C_5H_5)_3Ac(MW_5O_{19})_2]^{5-}$, Ac = U, Th and M = Nb, Ta: Day, V. W.; Klemperer, W. G.; Maltbie, D. J. *Organometallics* **1985**, *4*, 104.

(9) $HPV_2W_{10}O_{40}^{4-}$: Domaille, P. J.; Watunya, G. *Inorg. Chem.* **1986**, *25*, 1239.

(10) $H_2PV_3W_9O_{40}^{4-}$: see ref 9.

(11) $[[(C_5H_5)_2U]_2(TiW_5O_{19})_2]^{4-}$: Day, V. W.; Earley, C. W.; Klemperer, W. G.; Maltbie, D. J. *J. Am. Chem. Soc.* **1985**, *107*, 8261.

(12) $[M(Nb_6O_{19})_2]^{12-}$, M = Mn, Ni: (a) Dale, B. W.; Pope, M. T. *J. Chem. Soc., Chem. Commun.* **1967**, 792. (b) Flynn, C. M., Jr.; Stucky, G. D. *Inorg. Chem.* **1969**, *8*, 332. (c) Flynn, C. M., Jr.; Stucky, G. D. *Inorg. Chem.* **1969**, *8*, 335.

(13) $[(H_2O)(en)M(Nb_6O_{19})]^{5-}$, en = ethylenediamine and M = Cr, Co: Flynn, C. M., Jr.; Stucky, G. D. *Inorg. Chem.* **1969**, *8*, 178.

(14) $[(OC)_3M(Nb_2W_4O_{19})]^{3-}$, M = Mn, Re: (a) Besecker, C. J.; Klemperer, W. G. *J. Am. Chem. Soc.* **1980**, *102*, 7598. (b) Besecker, C. J.; Day, V. W.; Klemperer, W. G.; Thompson, M. R. *Inorg. Chem.* **1985**, *24*, 44.

(15) $\{[(CH_3)_5C_5]Rh(Nb_2W_4O_{19})\}^{2-}$: Besecker, C. J.; Day, V. W.; Klemperer, W. G.; Thompson, M. R. *J. Am. Chem. Soc.* **1984**, *106*, 4125.

(16) $[(C_5H_5)Ti(SiW_9V_3O_{40})]^{4-}$: (a) Finke, R. G.; Droege, M. W.; Cook, C. J.; Suslick, K. S. *J. Am. Chem. Soc.* **1984**, *106*, 5750. (b) Finke, R. G.; Rapko, B.; Domaille, P. J. *Organometallics* **1986**, *5*, 175.

(17) $\{[(CH_3)_5C_5]Rh(SiW_9Nb_3O_{40})\}^{5-}$: Finke, R. G.; Droege, M. W. *J. Am. Chem. Soc.* **1984**, *106*, 7274.

(18) $\{[(C_7H_8)Rh]_5(Nb_2W_4O_{19})_2\}^{3-}$: Besecker, C. J.; Klemperer, W. G.; Day, V. W. *J. Am. Chem. Soc.* **1982**, *104*, 6158.

(19) Day, V. W.; Klemperer, W. G.; Schwartz, C., manuscript in preparation.

0002-7863/87/1509-2991$01.50/0